

# STATISTICS ON RIEMANN ZEROS

RICARDO PÉREZ MARCO

## ABSTRACT

We numerically study the statistical properties of differences of zeros of Riemann zeta function and  $L$ -functions predicted by the theory of the  $\#$  product. In particular, this provides a simple algorithm that computes any non-real Riemann zeros from very large ones ("self-replicating property of Riemann zeros"). Also the algorithm computes the full sequence of non-real zeros of Riemann zeta function from the sequence of non-real zeros of any Dirichlet  $L$ -function ("zeros of  $L$ -functions know about Riemann zeros"). We also check that the first error to the convergence to the classical GUE statistic near 0 is a Fresnel distribution.

## CONTENTS

1. Introduction.	2
2. Self-replicating property of Riemann zeros.	4
3. Large Riemann zeros know about all zeros.	17
4. Zeros of $L$ -functions do know Riemann zeros.	20
5. Zeros of $L$ -functions replicate from their mating with Riemann zeros.	27
6. Mating of general $L$ -functions.	38
7. Mating with local Euler factors.	42
8. Fine structure of deltas near 0.	45
References	47

---

2000 *Mathematics Subject Classification.* 11M26.

*Key words and phrases.* Riemann zeta function,  $L$ -functions, zeros, statistics, distribution.

## 1. INTRODUCTION.

The goal of this article is to check numerically the predictions for the statistics of differences of zeros of Riemann zeta function and other  $L$ -functions anticipated by the theory of the eñe ring structure (see [PM1] and [PM2]). We carry out a detailed statistical analysis of the differences of zeros confirming the predicted limit distributions.

The study of the distribution for the differences of zeros is not new. In 1972 H.L. Montgomery ([Mo1], [Mo2]) investigated these statistics in relation with the class number problem. Although he states at the beginning of his article [Mo2] that

*"Our goal is to investigate the distribution of the differences  $\gamma - \gamma'$  between the zeros."*

he only studies this distribution for differences of nearby (consecutive or semi-locally close) zeros. Montgomery formulated the "Pair correlation conjecture" according to which, when  $T \rightarrow +\infty$ ,

$$\frac{1}{N(T)} \left| \left\{ (\gamma, \gamma'); \frac{2\pi\alpha}{\log T} < \gamma - \gamma' < \frac{2\pi\beta}{\log T} \right\} \right| \sim \int_{\alpha}^{\beta} \left( 1 - \left( \frac{\sin(\pi t)}{\pi t} \right)^2 \right) dt ,$$

where  $N(T) \sim \frac{1}{2\pi} T \log T$  is the asymptotic number of zeros with positive imaginary part less than  $T$ ,  $0 < \alpha < \beta$ , and the sum runs over the imaginary part of non-trivial Riemann zeros. Note the normalizing factor  $\frac{1}{2\pi} \log T$  that restricts the statistics to nearby zeros. According to the well known story, F. Dyson recognized the pair correlation distribution for eigenvalues of large random hermitian matrices used by physicists (the Gaussian Unitary Ensemble or GUE). This attracted much attention since it was believed to give some support to the spectral approach to the Riemann Hypothesis proposed by Hilbert and Polya (indeed first by Polya according to [Od]), which asks to identify an hermitian operator whose spectrum is composed by the non-real Riemann zeros (this belief is not justified as we will discuss later on).

Then in the 80's A.M. Odlyzko performed intensive computations of the distribution of normalized differences of consecutive Riemann zeros confirming numerically the GUE distribution conjectured by Montgomery ([Od]). Later N. Katz and P. Sarnak pursued the numerical exploration of zeros for other  $L$ -functions ([KS]). Their work was continued more recently by many others (see [Co]).

These authors restrict their study to normalized differences of consecutive zeros. Our goal is to study the distribution of global differences at large. These global differences appear on compact sets uniformly distributed in first approximation. At the second order they present very significant discrepancies with the uniform distribution

(section 2). The precise location of these discrepancies is highly significant: We notice a deficiency of differences of non-real Riemann zeros exactly and precisely at the same locations as the Riemann zeros. In other words, the statistics of differences of Riemann zeros pinpoints the exact location of these zeros.

In particular, this property indicates that large Riemann zeros do know the location of all Riemann zeros, since the statistics remain unchanged by removing a finite number (or a density 0 subset) of Riemann zeros. It is indeed checked numerically in section 3 that the statistics of very large zeros do find the location the first Riemann zeros.

We also study the differences of the zeros of an arbitrary Dirichlet  $L$ -function (section 4). We observe the same phenomenon. The differences have a uniform distribution except for deficits located exactly at the precise location of Riemann zeros. This fact provides a simple algorithm which computes the sequence of Riemann zeros from the sequence of zeros of any Dirichlet  $L$ -function. This result confirms what has been part of the folklore intuition among the community of specialists (see [Co]): Zeros of  $L$ -functions do know about Riemann zeros.

We perform a statistics in sections 5 and 6 which is apparently new in the literature. We study the differences of the zeros of one Dirichlet  $L$ -function  $L_1$  against the zeros of another Dirichlet  $L$ -function  $L_2$ . A similar result is observed: The discrepancies from the uniform distribution are located at the zeros of another  $L$ -function which can be computed explicitly. When  $L_2$  is the Riemann zeta function (section 6), the discrepancies are located at the zeros of  $L_1$ , i.e. Riemann's zeta function plays the role of the identity for this mating operation. In section 7, we mate local Euler factors with Riemann zeta function. The discrepancies pinpoint to the arithmetic location of the poles of the Euler factor.

We also make a numerical study of the distribution predicted by Montgomery's conjecture (section 8). The theory of the  $\text{e}\tilde{\text{n}}\text{e}$  product provides a refinement of Montgomery's conjecture. More precisely, it provides, and we verify numerically, an asymptotics for the error from Montgomery's GUE limit distribution. At the first order we observe the predicted Fresnel (or sine cardinal) distribution. These refinements of Montgomery's conjecture seem also new.

The numerical results presented in this article are unexpected without the theory of the  $\text{e}\tilde{\text{n}}\text{e}$  product. Even more surprising is that such elementary statistics have been unnoticed so far. We encourage the skeptic readers who want to "put their hand upon the wound" to check the numerical results by themselves in their own personal computer (any modern personal computer can do the job). It is indeed extremely

simple as we indicate below. All statistics presented in this article were performed with public software and public data on a low profile regular laptop (of 2005, with 500 Mb of RAM memory). They are fully reproducible and we provide all necessary information to reproduce them.

Together with the numerical results we give the simple code for the computations. These were performed using the public domain statistical software "R". One can download and install the program from the site [www.r-project.org](http://www.r-project.org) where tutorials are also available. This statistical software runs under Linux and Windows and the source code is open. Some source files for zeros of the Riemann zeta function were obtained from A. M. Odlyzko's web site [Od]. A large source file for the 35 first million non-trivial Riemann zeros and other files with zeros of  $L$ -functions are from M. Rubinstein public site [Ru]. The author is very grateful to A.M. Odlyzko and M. Rubinstein for making available their data.

We have restricted our statistics to Dirichlet  $L$ -functions only because we have only access to large lists of zeros for these functions. These results hold in general for more general  $L$  and zeta functions. We encourage the readers with access to zero data for other more general  $L$ -functions to perform similar statistics.

From now on we refer to non-real zeros of Riemann's zeta function simply as "zeros of Riemann's zeta function" or "Riemann zeros". The same simplified terminology is used for non-real zeros of general  $L$ -functions. We also refer to differences as "deltas". We use the notation  $\rho$  for a non-real zero and the notation  $\gamma$  for  $\rho = 1/2 + i\gamma$ . Then the sequence of  $\gamma$ 's is the sequence of non-trivial zeros of Riemann real analytic function on the vertical line  $\{\Re s = 1/2\}$ . We eventually refer to them also as Riemann zeros.

### Acknowledgments.

These numerical computations were conducted during 2004 and 2005, and this manuscript was written in 2005. It was circulated among some close friends. I am very grateful for their support during these years. These results were announced in the conference in Honor of the 200th birthday of Galois, "Differential Equations and Galois Theory", held at I.H.E.S. in October 2011.

## 2. SELF-REPLICATING PROPERTY OF RIEMANN ZEROS.

We consider the sequence  $\mathcal{Z} = (\rho_i)_{i \geq 1}$  of Riemann's zeros with positive imaginary part. We label them in increasing order,  $\Im \rho_i > \Im \rho_j$  for  $i > j$ . We write  $\rho_j = 1/2 + i\gamma_j$ . The first few zeros were computed by B. Riemann with high accuracy as was found in Riemann's Nachlass ([Ri2]). The tabulation of the first 80 zeros, i.e. all zeros less than 200 follows:

$$\begin{aligned}\gamma_1 &= 14.134725142 \dots \\ \gamma_2 &= 21.022039639 \dots \\ \gamma_3 &= 25.010857580 \dots \\ \gamma_4 &= 30.424876126 \dots \\ \gamma_5 &= 32.935061588 \dots \\ \gamma_6 &= 37.586178159 \dots \\ \gamma_7 &= 40.918719012 \dots \\ \gamma_8 &= 43.327073281 \dots \\ \gamma_9 &= 48.005150881 \dots \\ \gamma_{10} &= 49.773832478 \dots \\ \gamma_{11} &= 52.970321478 \dots \\ \gamma_{12} &= 56.446247697 \dots \\ \gamma_{13} &= 59.347044003 \dots \\ \gamma_{14} &= 60.831778525 \dots \\ \gamma_{15} &= 65.112544048 \dots \\ \gamma_{16} &= 67.079810529 \dots \\ \gamma_{17} &= 69.546401711 \dots \\ \gamma_{18} &= 72.067157674 \dots \\ \gamma_{19} &= 75.704690699 \dots \\ \gamma_{20} &= 77.144840069 \dots \\ \gamma_{21} &= 79.337375020 \dots \\ \gamma_{22} &= 82.910380854 \dots \\ \gamma_{23} &= 84.735492981 \dots \\ \gamma_{24} &= 87.425274613 \dots \\ \gamma_{25} &= 88.809111208 \dots \\ \gamma_{26} &= 92.491899271 \dots \\ \gamma_{27} &= 94.651344041 \dots \\ \gamma_{28} &= 95.870634228 \dots \\ \gamma_{29} &= 98.831194218 \dots \\ \gamma_{30} &= 101.317851006 \dots \\ \gamma_{31} &= 103.725538040 \dots \\ \gamma_{32} &= 105.446623052 \dots \\ \gamma_{33} &= 107.168611184 \dots \\ \gamma_{34} &= 111.029535543 \dots \\ \gamma_{35} &= 111.874659177 \dots \\ \gamma_{36} &= 114.320220915 \dots \\ \gamma_{37} &= 116.226680321 \dots\end{aligned}$$

$$\begin{aligned}\gamma_{38} &= 118.790782866 \dots \\ \gamma_{39} &= 121.370125002 \dots \\ \gamma_{40} &= 122.946829294 \dots \\ \gamma_{41} &= 124.256818554 \dots \\ \gamma_{42} &= 127.516683880 \dots \\ \gamma_{43} &= 129.578704200 \dots \\ \gamma_{44} &= 131.087688531 \dots \\ \gamma_{45} &= 133.497737203 \dots \\ \gamma_{46} &= 134.756509753 \dots \\ \gamma_{47} &= 138.116042055 \dots \\ \gamma_{48} &= 139.736208952 \dots \\ \gamma_{49} &= 141.123707404 \dots \\ \gamma_{50} &= 143.111845808 \dots \\ \gamma_{51} &= 146.000982487 \dots \\ \gamma_{52} &= 147.422765343 \dots \\ \gamma_{53} &= 150.053520421 \dots \\ \gamma_{54} &= 150.925257612 \dots \\ \gamma_{55} &= 153.024693811 \dots \\ \gamma_{56} &= 156.112909294 \dots \\ \gamma_{57} &= 157.597591818 \dots \\ \gamma_{58} &= 158.849988171 \dots \\ \gamma_{59} &= 161.188964138 \dots \\ \gamma_{60} &= 163.030709687 \dots \\ \gamma_{61} &= 165.537069188 \dots \\ \gamma_{62} &= 167.184439978 \dots \\ \gamma_{63} &= 169.094515416 \dots \\ \gamma_{64} &= 169.911976479 \dots \\ \gamma_{65} &= 173.411536520 \dots \\ \gamma_{66} &= 174.754191523 \dots \\ \gamma_{67} &= 176.441434298 \dots \\ \gamma_{68} &= 178.377407776 \dots \\ \gamma_{69} &= 179.916484020 \dots \\ \gamma_{70} &= 182.207078484 \dots \\ \gamma_{71} &= 184.874467848 \dots \\ \gamma_{72} &= 185.598783678 \dots \\ \gamma_{73} &= 187.228922584 \dots \\ \gamma_{74} &= 189.416158656 \dots\end{aligned}$$

$$\begin{aligned}
\gamma_{75} &= 192.026656361 \dots \\
\gamma_{76} &= 193.079726604 \dots \\
\gamma_{77} &= 195.265396680 \dots \\
\gamma_{79} &= 196.876481841 \dots \\
\gamma_{80} &= 198.015309676 \dots \\
&\vdots
\end{aligned}$$

We use the notation, for  $1 \leq j < i$ ,

$$\delta_{i,j} = \gamma_i - \gamma_j .$$

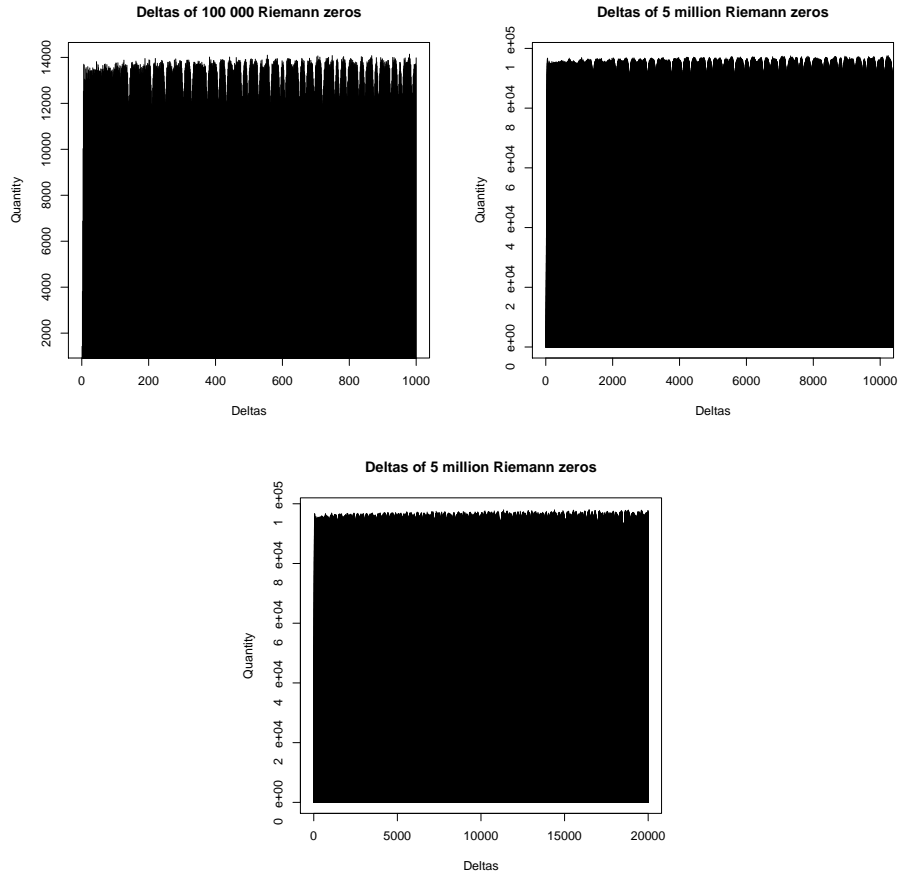
We fix  $N > 0$ . Given  $T > 0$  we consider the subset of all deltas of zeros:

$$\Delta_{T,N} = \{0 < \delta_{i,j} \leq T; 1 \leq j < i \leq N\} \subset ]0, T]$$

We denote by  $T_0 = \gamma_N$  and  $N = N(T_0)$ . We are interested in the numerical study of the distribution of the elements of  $\Delta_{T,N}$  when  $N \rightarrow +\infty$  and  $T > 0$  is kept fixed.

We represent the histogram of values in  $\Delta_{T,N}$  by ticks of  $\epsilon = 10^{-m}$  for some  $T > 0$  and  $N$  large. That is, for each integer  $1 \leq k \leq 1 + T\epsilon^{-1}$  we count how many deltas  $\delta$  yield  $k = \lceil \epsilon^{-1}\delta \rceil$  (here the brackets denote the integer part). We denote by  $x_k \geq 0$  this number. The histograms represent the sequence  $(x_k)_{1 \leq k \leq 1 + T\epsilon^{-1}}$ . We represent the figures obtained from two statistics. One very fast and the second more intensive and precise. The first one, named (a), computes the deltas of  $N = 10^5$  zeros with precision  $\epsilon = 10^{-1}$  and  $T = 100$ . The computation takes about 15 minutes on the author's laptop. The statistics named (b) computes the deltas for  $N = 5 \cdot 10^6$  with precision  $\epsilon = 10^{-2}$  and  $T = 200$ . This computation took about 2 days on the author's laptop. Obviously, reducing  $T$  or increasing  $\epsilon$  greatly diminishes the computation time.

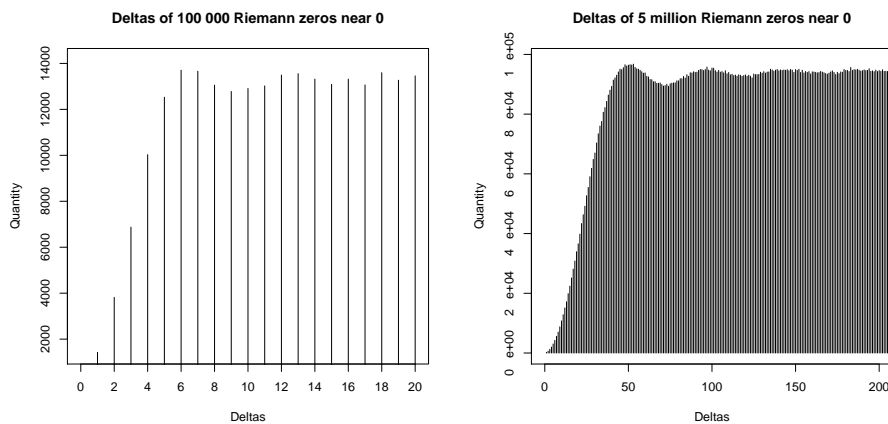
Figure 1.a represents the histogram for statistics (a). Figure 1.b represents the histogram for statistic (b), restricted to the range  $[0, 100]$ . Figure 1.c represents the histogram for statistic (b) in the full range  $[0, 200]$ .



Figures 1.a, 1.b and 1.c.

At first sight this distribution seems to converge (once properly normalized) weakly to the uniform distribution on  $[0, T]$ . This uniformity for the statistics of global deltas of zeros (i.e. non-consecutive) does not seem to have been noted explicitly in the literature. It is hinted by the tail asymptotic to density 1 of Montgomery's pair correlation distribution, but it doesn't follow from that due to the semi-locality of the differences. We discuss this later in more detail.

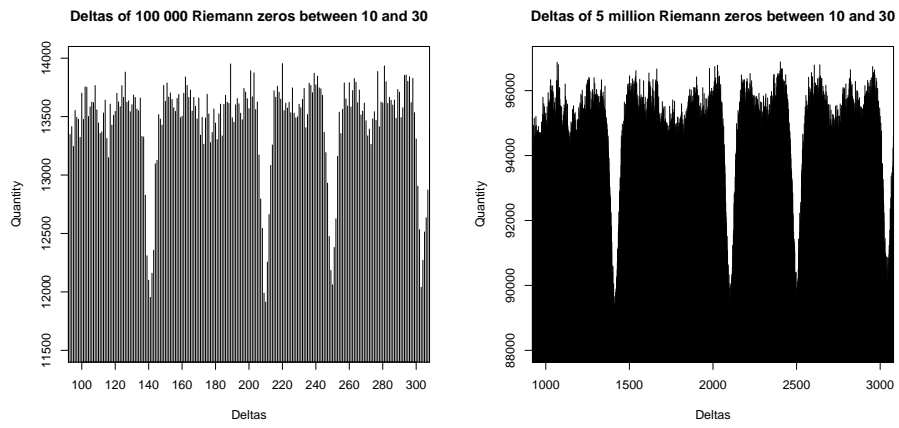
But a closer look to the histogram shows some divergence to the uniform distribution. The convergence does not appear to be uniform on  $[0, T]$ . We can notice one major deficiency for small deltas. This appears when we zoom in the picture near 0 (see figures 2.a and 2.b for the range of deltas  $[0, 2]$ ).



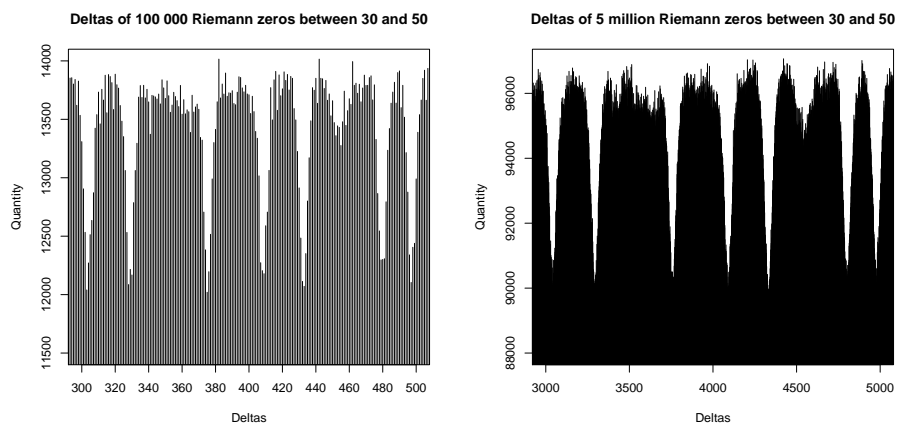
Figures 2.a and 2.b.

This deficiency is related to the observed fact that the GUE pair correlation distribution implies that consecutive zeros tend to repel each other. A closer look at the figures reveals a compressed scaled GUE pair correlation distribution as expected. The factor of compression is  $\frac{1}{2\pi} \log T_0$  as one should expect from Montgomery’s conjecture. Notice that scaling the figures by the factor  $\frac{1}{2\pi} \log T_0$  (as done by those authors studying numerically Montgomery’s conjectures) pushes away to  $+\infty$  (when  $T_0 \rightarrow +\infty$  and  $N \rightarrow +\infty$ ) all the other interesting irregularities of the histogram that are the focus of our study.

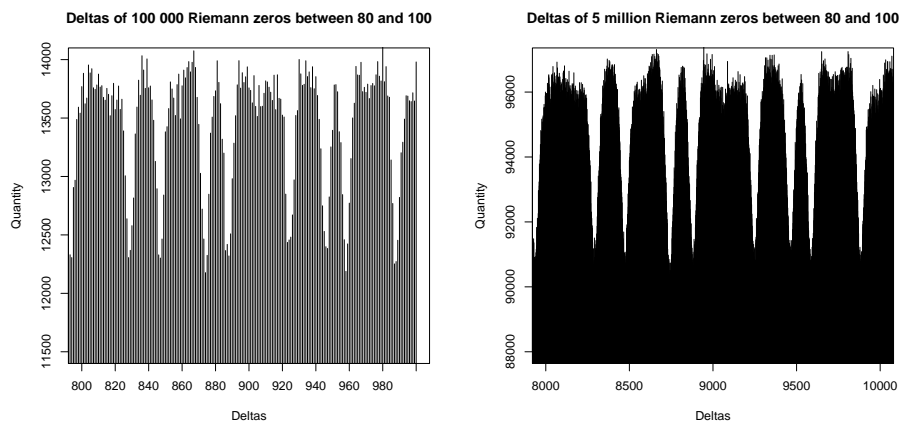
Indeed, other divergences to the uniform distribution appear at some special places distinct from 0. We notice a remarkable deficit of deltas at certain locations. This can be seen clearly by zooming in at several places. Figures 3.a and 3.b shows zooms at the interval  $[10.00, 30.00]$ . Figures 4.a and 4.b are centered at the interval  $[30.00, 50.00]$ . Figure 5.a and 5.b at the interval  $[80.00, 100.00]$ . In all these pictures we observe at certain precise locations noticeable negative spikes, i.e. a well localized deficit of deltas.



Figures 3.a and 3.b.

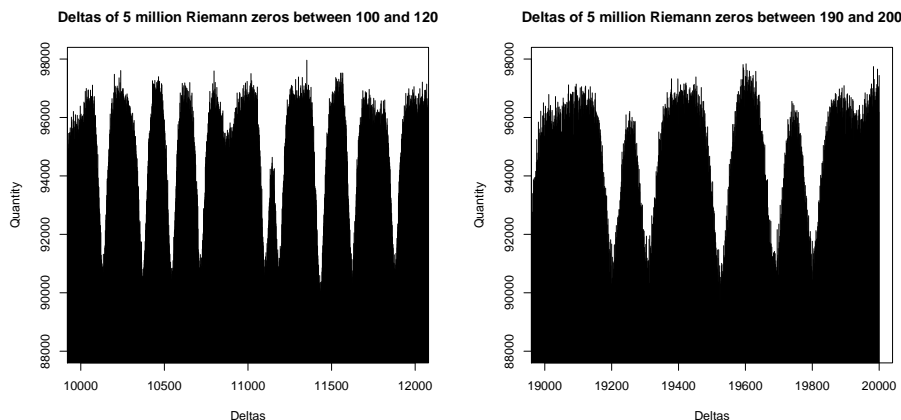


Figures 4.a and 4.b.



Figures 5.a and 5.b.

For statistics (b) with  $T = 200$  we can check larger intervals. Figures 6 and 7 are centered around the intervals  $[100.00, 120.00]$  and  $[190.00, 200.00]$ .



Figures 6 and 7. Statistics (b).

At this point the reader should take a moment and compare these pictures, and in particular the location of the deficiencies, with the tabulated list of Riemann zeros.

The key observation now is that the location of these negative spikes is truly special. These locations are precisely at the very same location of the Riemann zeros. We recognize in figures 3.a and 3.b the locations of the 4 first Riemann zeros. In all the Figures 3a, 3b, 4a, 4b, 5a, 5b, 6 and 7 we recognize the location of the zeros in the corresponding intervals. Note in particular in figure 6 the two nearby zeros near the value 111,

$$\gamma_{34} = 111.029535543\dots \quad \gamma_{35} = 111.874659177\dots$$

We conclude that

**Riemann zeros do repel their deltas.**

This property of the sequence of Riemann zeros is even more surprising considering the fact that it is not invariant by translation, i.e. by a global translation of the sequence. The set of deltas is independent of such a translation, but obviously not this property. The location of each zero is well determined. Any variation on the location of a single zero is obviously irrelevant for the distribution of deltas, but the zero will then miss the location of the negative spike. Therefore, only the statistics of the deltas determines the precise location of the zeros. This implies that **any subsequence of density 1 of Riemann zeros does determine the whole sequence**. For this reason we name this property **the self replicating property of the zeros**.

The self replicating property of the Riemann zeros is completely mysterious without the motivation that lies behind this numerical study: The theory of the eñe product.

We can confirm numerically these observations (in statistics (a) for simplicity) by noticing that in the histogram all the deficit values with cumulative count inferior to 12 500 fall near a Riemann zero, and conversely any Riemann zero yields a group of deficit values. The list of the values of  $k$  for which  $x_k < 12\,500$  in statistics (a) is the following: 1, 2, 3, 4, 5, 139, 140, 141, 142, 143, 208, 209, 210, 211, 212, 248, 249, 250, 251, 252, 302, 303, 304, 305, 306, 327, 328, 329, 330, 374, 375, 376, 377, 407, 408, 409, 410, 431, 432, 433, 434, 478, 479, 480, 481, 496, 497, 498, 499, 528, 529, 530, 531, 563, 564, 565, 566, 592, 593, 594, 606, 607, 608, 609, 649, 650, 651, 652, 669, 670, 671, 694, 695, 696, 718, 719, 720, 721, 722, 755, 756, 757, 758, 770, 771, 772, 792, 793, 794, 827, 828, 829, 830, 846, 847, 848, 873, 874, 875, 886, 887, 888, 889, 923, 924, 925, 945, 946, 947, 957, 958, 959, 987, 988, 989.

To make the main observation more precise, we can, for example, average out all deficit values in each group. We discard the first group of values near 0 that corresponds to the deficit at 0 (we will come back to this). Then we find out as many groups as Riemann zeros and their averages are denoted by  $\bar{\gamma}_1, \bar{\gamma}_2, \bar{\gamma}_3, \dots$ . They are all very close to the corresponding zero. Table 6 compares the sequence of zeros ( $\gamma_i$ ) with the sequence of averages ( $\bar{\gamma}_i$ ) for all 29 zeros less than 100. We rounded up the averages to the first decimal. The matching of the averages  $\bar{\gamma}$  with the zeros  $\gamma$  is striking.

i	$\gamma_i$	$\bar{\gamma}_i$
1	14.134725142	14.1
2	21.022039639	21.0
3	25.010857580	25.0
4	30.424876126	30.4
5	32.935061588	32.9
6	37.586178159	37.6
7	40.918719012	40.9
8	43.327073281	43.3
9	48.005150881	48.0
10	49.773832478	49.8
11	52.970321478	53.0
12	56.446247697	56.5
13	59.347044003	59.3
14	60.831778525	60.8
15	65.112544048	65.1
16	67.079810529	67.0
17	69.546401711	69.5
18	72.067157674	72.0
19	75.704690699	75.7
20	77.144840069	77.1
21	79.337375020	79.3
22	82.910380854	82.9
23	84.735492981	84.7
24	87.425274613	87.4
25	88.809111208	88.8
26	92.491899271	92.4
27	94.651344041	94.6
28	95.870634228	95.8
29	98.831194218	98.8

### Zeros versus group averages.

It is also interesting to study the structure of the distribution of the deficit of deltas near the zeros. Once properly scaled, we observe a universal distribution for all zeros. This distribution is a negative Fresnel distribution, i.e. the distribution generated by the Fresnel integral (also named sine integral, or sine cardinal function)

$$\operatorname{sinc}_\pi(x) = \begin{cases} \frac{\sin(\pi x)}{\pi x} & \text{for } x \neq 0 \\ 1 & \text{for } x = 0 \end{cases}$$

We have

$$\int_{-\infty}^{+\infty} \operatorname{sinc}_{\pi}(x) dx = 1 .$$

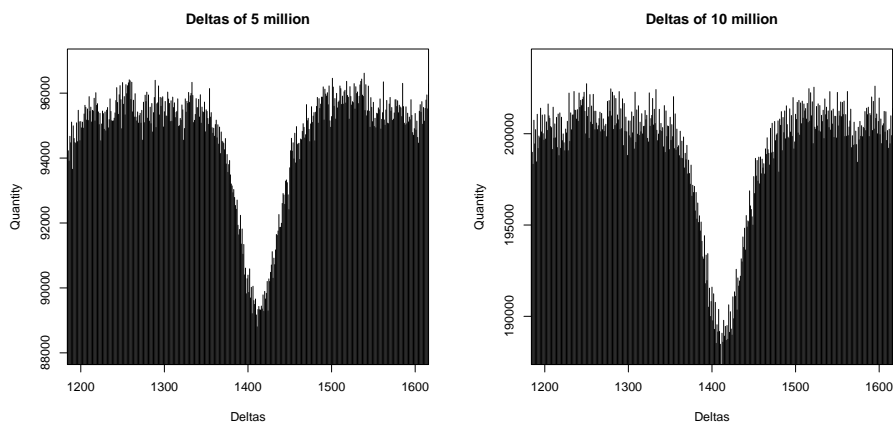
The Fresnel distribution is the Fourier transform

$$\operatorname{sinc}_{\pi}(x) = \int_{\mathbb{R}} e^{-2\pi ixt} \Pi(t) dt ,$$

of the box function,

$$\Pi(x) = H(x + 1/2) - H(x - 1/2) = \begin{cases} 0 & \text{for } |x| > 1/2 , \\ 1 & \text{for } |x| < 1/2 . \end{cases}$$

We can appreciate this for the histogram plotted in Figure 8.a. Figure 8.b shows a more intensive computation with deltas of the first 10 million zeros.

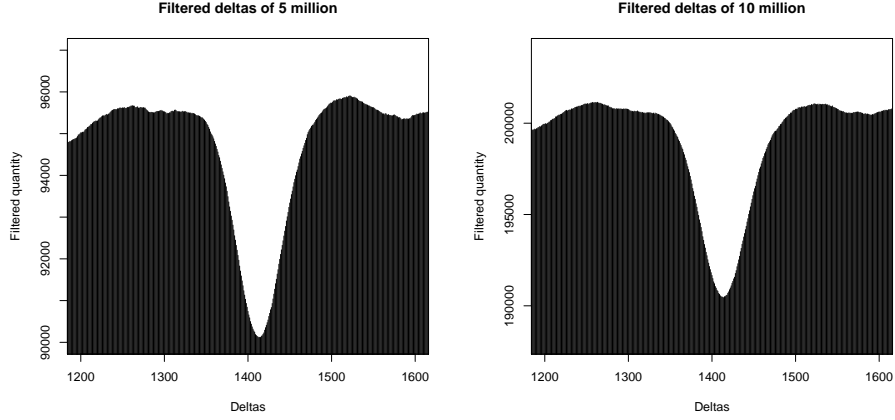


Figures 8.a and 8.b.

In the figures we appreciate a higher frequency noise that blurs the picture. We can filter the noise out by standard filtering procedures. The simplest one would be to replace (for example) the sequence  $(x_k)$  by the sequence  $(fx_k)$  where

$$fx_k = \frac{1}{\tau} \sum_{i=-\tau/2}^{\tau/2} x_k .$$

The new figures 9.a and 9.b show the pictures with the noise filtered.



Figures 9.a and 9.b.

**Eñe product computation.**

These numerical observations come from the analytic divisor interpretation of the eñe product, noted  $\bar{\star}$ , developed in [PM1] and [PM2]. The space of Dirichlet  $L$ -functions endowed with usual the multiplication and the eñe product is a commutative ring, having a proper normalization of the Riemann zeta function as the eñe-multiplicative unit. The eñe product is associative, not only with respect to multiplication, but also to infinite arithmetic Euler products. Given two Euler products with polynomials  $(F_p)$  and  $(G_p)$  (with  $F_p(0) = G_p(0) = 1$ ),

$$F(s) = \prod_p F_p(p^{-s})$$

$$G(s) = \prod_p G_p(p^{-s})$$

then

$$F \bar{\star} G(s) = \prod_p F_p \star G_p(p^{-s}) ,$$

where  $F_p \star G_p$  is the plain eñe product in  $\mathbb{C}$  of polynomial whose zeros are the product of the zeros of  $F_p$  with the zeros of  $G_p$ , i.e. if

$$F_p(X) = \prod_{\alpha} \left(1 - \frac{X}{\alpha}\right)$$

$$G_p(X) = \prod_{\beta} \left(1 - \frac{X}{\beta}\right)$$

then

$$F_p \star G_p = \prod_{\alpha, \beta} \left( 1 - \frac{X}{\alpha\beta} \right) ,$$

in particular

$$(1 - ap^{-s}) \bar{\star} (1 - bp^{-s}) = 1 - abp^{-s} .$$

The main arithmetic property is that for  $p \neq q$ , we have  $\log p$  and  $\log q$   $\mathbb{Q}$ -independent, and

$$F_p(p^{-s}) \bar{\star} G_q(q^{-s}) = 1 .$$

Now we denote that for a real analytic function  $F$ ,

$$\bar{F}(s) = \overline{F(\bar{s})} = F(s) .$$

The main statistics in this section have its origin in the following computation

$$\begin{aligned} \zeta(s) \bar{\star} \bar{\zeta}(s) &= \zeta(s) \bar{\star} \zeta(s) \\ &= \left( \prod_p (1 - p^{-s})^{-1} \right) \bar{\star} \left( \prod_q (1 - q^{-s})^{-1} \right) \\ &= \prod_p (1 - p^{-s})^{-1} \bar{\star} (1 - p^{-s})^{-1} \\ &= \prod_p (1 - p^{-1/2} p^{-s}) \\ &= \zeta(s + 1/2)^{-1} . \end{aligned}$$

### R script.

The following script can be directly feeded into R in order to plot the histogram for the deltas for 5 million zeros with precision  $10^{-2}$  (statistics (b)). The zeros are read from the file "zero.data" (one zero per line in increasing order). The reader can consult the R tutorial for more elaborate plotting commands. The scripts for the other statistics are simple modifications from this one.

```
zero1<-scan("zero.data", nlines=5000000)
zero2<-zeta1
x=rep(0,10000)
N=5000000
k=0
for (i in 1:N)
{
```

```

while (((zero1[i]-zero2[i+k])<100.01) & (k+i>1))
{
k<-k-1
}
k=k+1
j=k
while ( (zero1[i]-zero2[i+j]>0) & (zero1[i]-zero2[i+j]<100.01) )
{
d=100*(zero1[i]-zero2[i+j]) x[as.integer(d)]=x[as.integer(d)]+1
j=j+1
}
}
barplot(x)

```

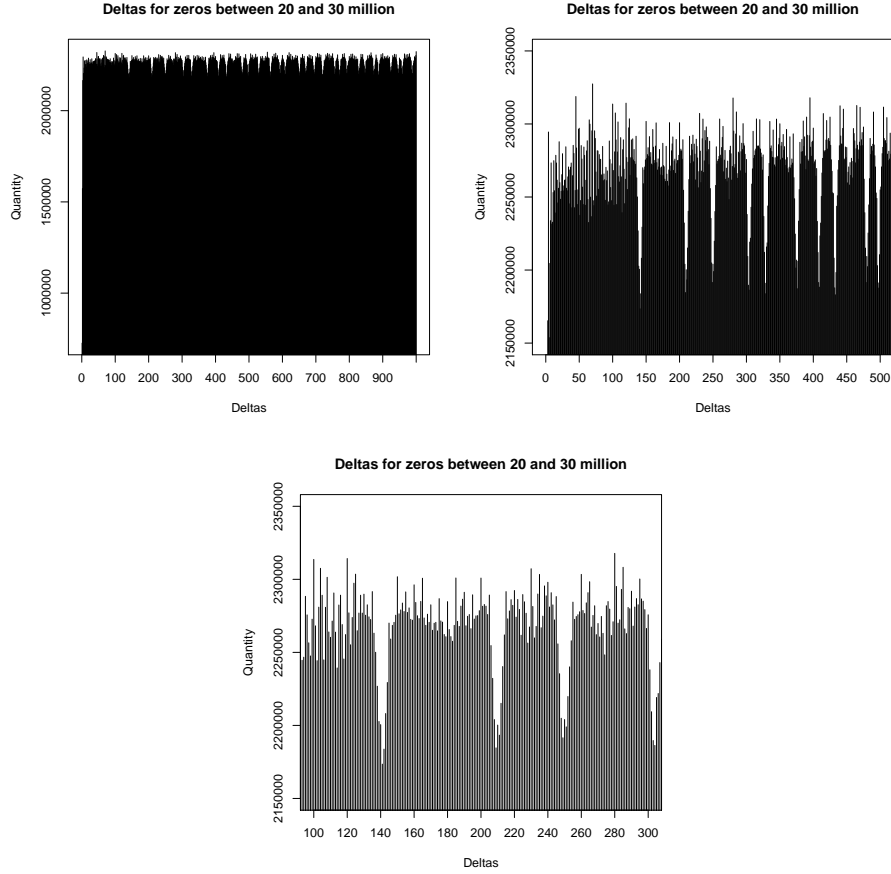
### 3. LARGE RIEMANN ZEROS KNOW ABOUT ALL ZEROS.

In this section we perform the same statistics as in section 1, but only using deltas of large zeros. The convergence is slower, but the results are the same. This indicates that zeros with large imaginary part contain full information on the location of all zeros. Indeed a density 1 proportion of zeros with large imaginary part contains the information about the location of all zeros.

We perform the statistics with two sets of data. The first one, using Rubinstein's file for the first 35 million zeros and selecting one million after the 30th million zero. The second and the third are performed with a much larger set of zeros using Odlyzko's file containing 10 000 zeros after  $10^{12}$  and after  $10^{21}$  respectively. The number of zeros in these last two statistics is insufficient. These sets of 10 000 zeros are small and the distribution of deltas is not even close to the uniform distribution. In the first Odlyzko's file all deltas are smaller than 2568 and in the second smaller than 1409. Therefore we observe a linear deficit of deltas even for small values of delta when delta increases. In order to pinpoint the deficit at the zeros we filter the cumulative data on deltas by removing a moving average. Although statistically not as significant as the other statistics, the deficit phenomena is still clearly visible at the location of the zeros. It is also less visible for large zeros. This indicates a slower convergence.

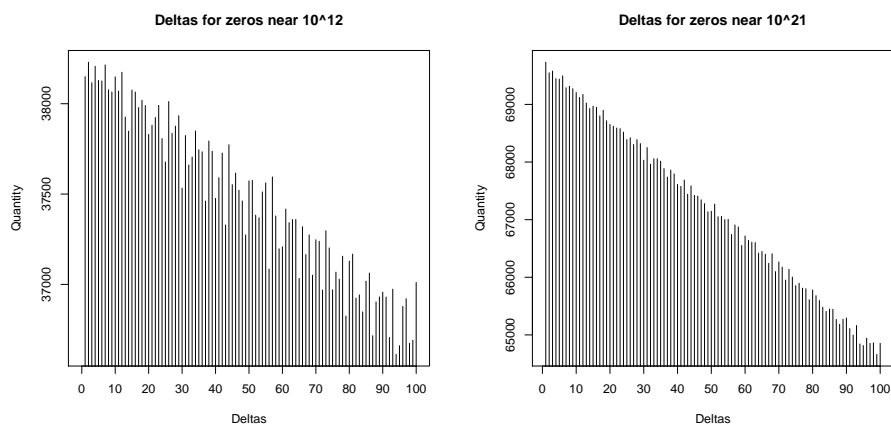
The following figures 10a, 10b and 10c are from the first statistics with 10 million zeros ( $\gamma_i$ ) with  $20.10^6 < i \leq 30.10^6$ . Figures 10b and 10c show the details near the top of the uniform distribution. We can appreciate the similarity of these pictures

with the previous ones. Figure 10c is centered around the segment  $[10, 30]$  and is almost identical to figures 3a and 3b.

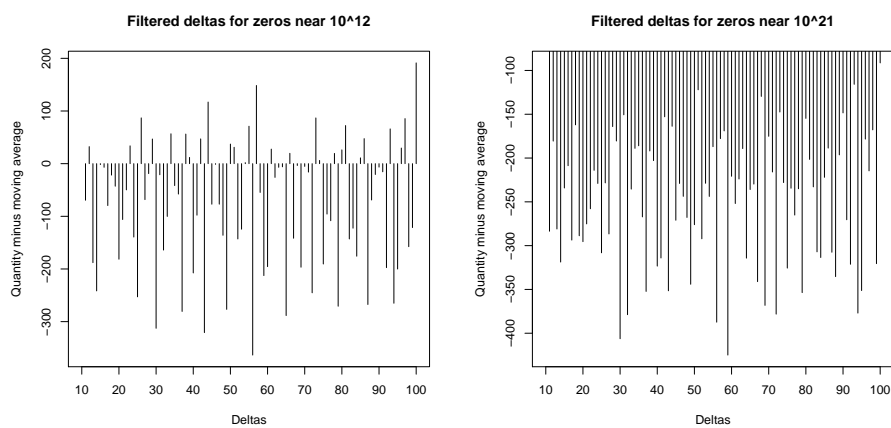


Figures 10.a, 10.b and 10.c.

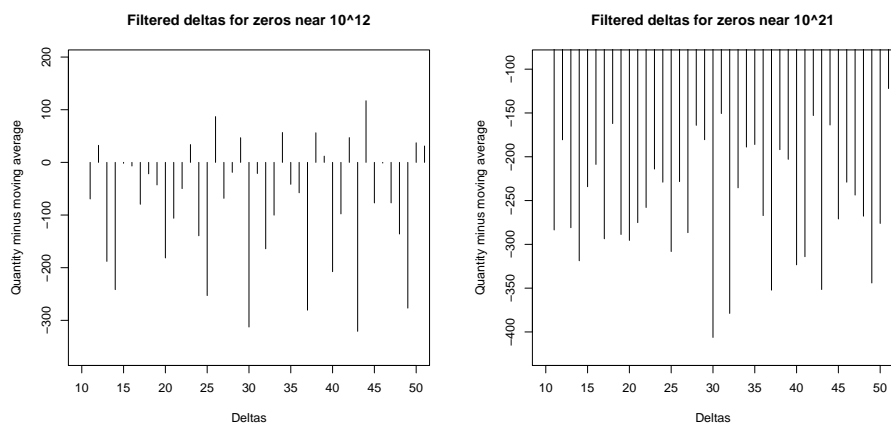
In the following figures we illustrate the results for Odlyzko's large zeros near  $10^{12}$  (statistics (a)) and near  $10^{21}$  (statistics (b)). We can observe the linear decreasing of the amount of deltas due to the small number of zeros used. We worked with Odlyzko's files containing only 10 000 zeros. Paying close attention we can discern the deficit of deltas at the location of the zeros. This can be better seen by filtering the data by removing a moving average. Figures 12.a and 12.b show that. In Figures 13.a and 13.b we have the details for deltas smaller than 50.



Figures 11.a and 11.b.



Figures 12.a and 12.b.



Figures 13.a and 13.b.

4. ZEROS OF  $L$ -FUNCTIONS DO KNOW RIEMANN ZEROS.

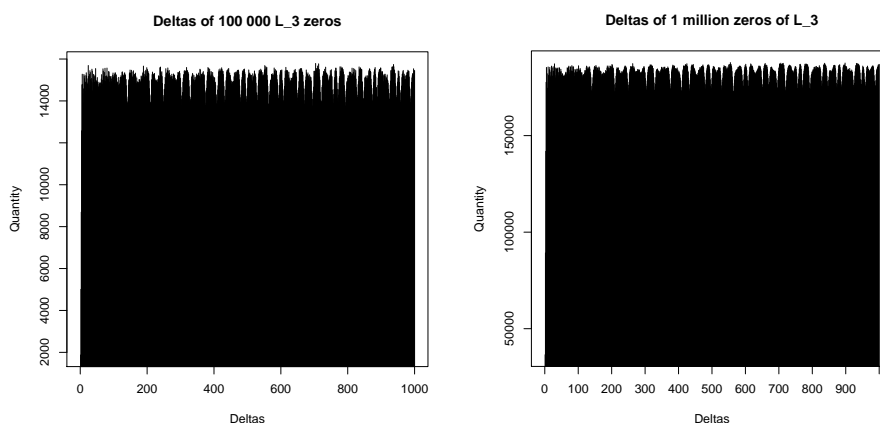
In the survey article of B. Conrey on the Riemann Hypothesis ([Co]) we can read in the section entitled "The conspiracy of  $L$ -functions",

*There is a growing body of evidence that there is a conspiracy among  $L$ -functions (...) The first clue that zeta- and  $L$ -functions even know about each other appears perhaps in works of Deuring and Heilbronn (...) These results together (...) gave the first indication of a connection between the zeros of  $\zeta(s)$  and those of  $L(s, \chi_d)$ .*

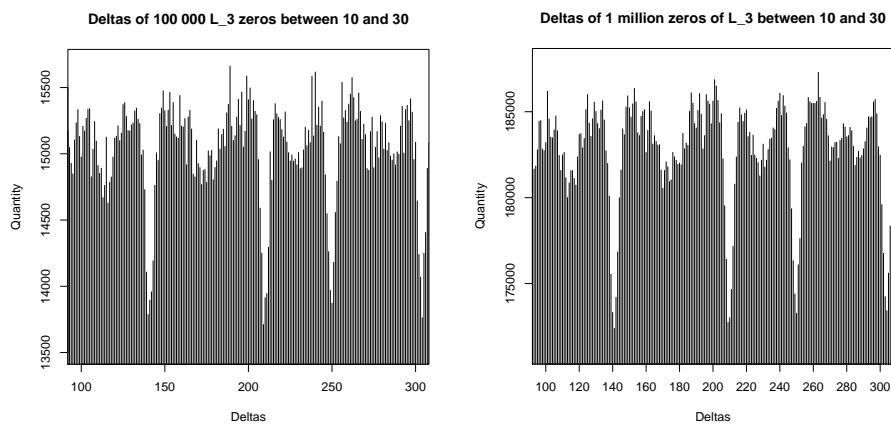
We confirm in this section that zeros of  $L$ -functions do know about all Riemann zeros. Indeed we provide a simple algorithm that builds the sequence of Riemann zeros from the sequence of zeros of any Dirichlet  $L$ -functions. Our first example is for the simplest non-trivial  $L$ -function: We show how to recover Riemann zeros from the zeros of  $L_{\chi_3}$ , where  $\chi_3$  is the only character of conductor 3.

We perform the statistics for the deltas of the zeros of  $L_{\chi_3}$  as done in section 2 for Riemann zeros. This time we observe that the deficit values for the deltas of zeros of  $L_{\chi_3}$  is located precisely at Riemann zeros. As in section 2 we perform one statistic with 100 000 zeros of  $L_{\chi_3}$  and precision 0.1 for the deltas, and another, more intensive, with 5 million zeros of  $L_{\chi_3}$ . Figures 14 show the histogram of deltas for both statistics. Figures 15 show the details in the interval  $[10, 30]$ , figures 16 for  $[30, 50]$ , and figures 17 for  $[80, 100]$ . We observe in figures 18 the deficit of deltas near 0 verifying Montgomery's prediction.

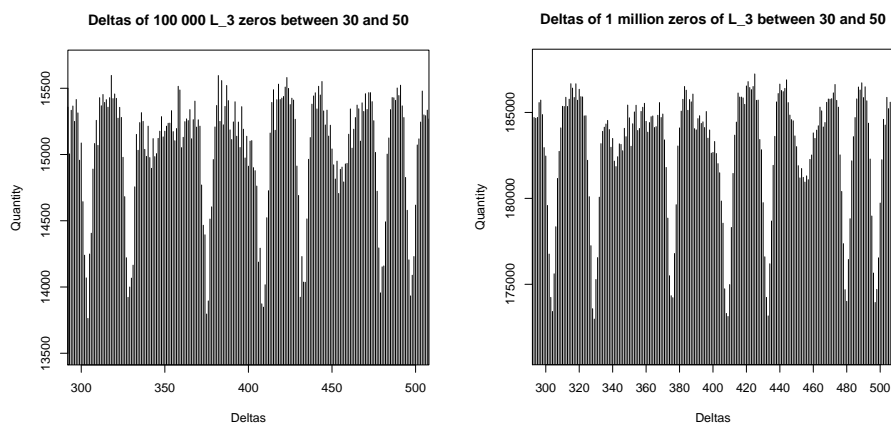
The similarity of these figures with those in section 2 is clear. Recall though that they are generated from a very different set of data.



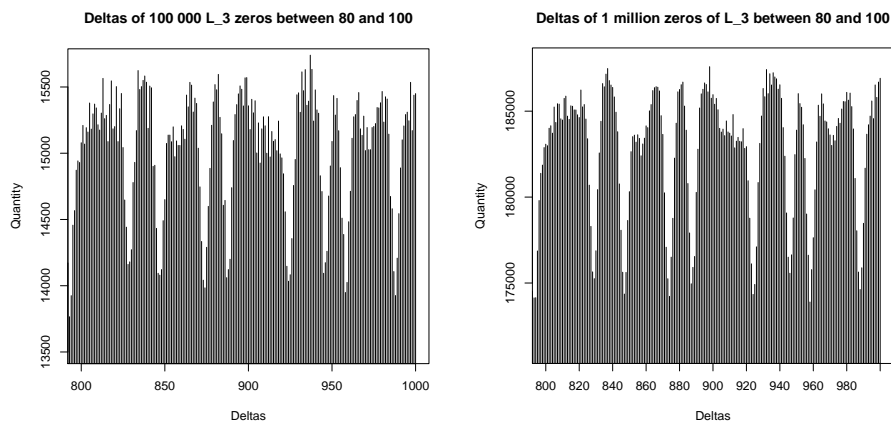
Figures 14.a and 14.b.



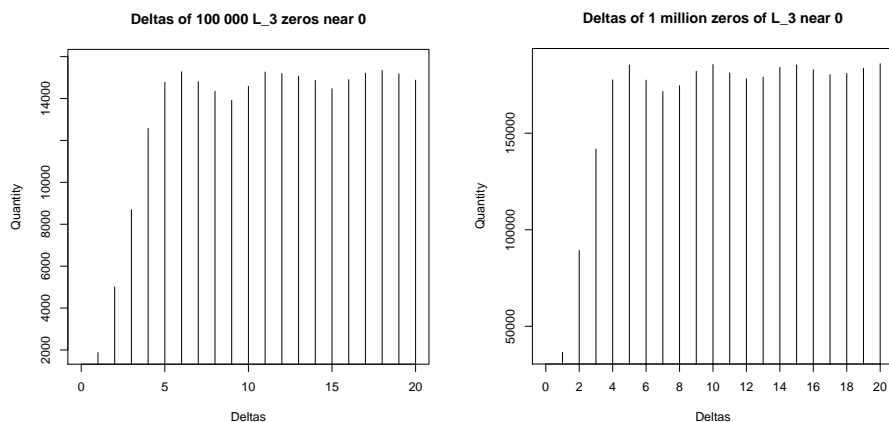
Figures 15.a and 15.b.



Figures 16.a and 16.b.



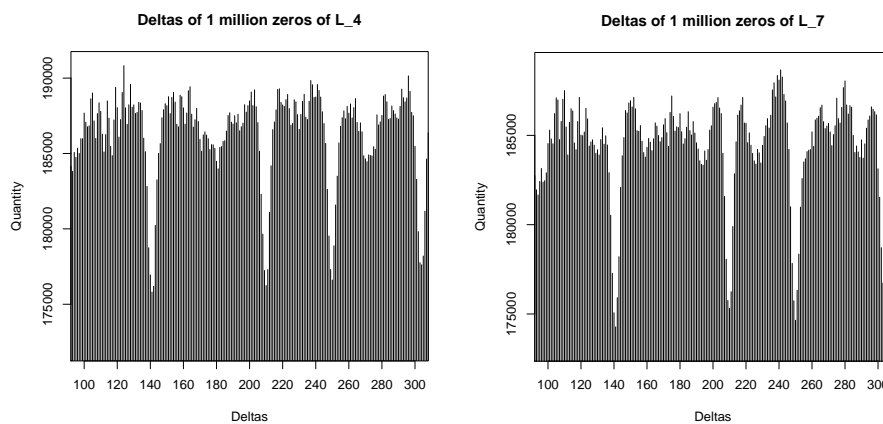
Figures 17.a and 17.b.



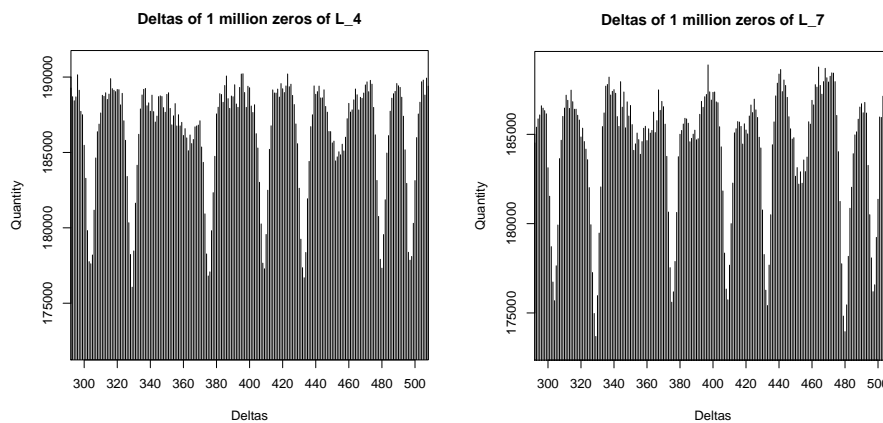
Figures 18.a and 18.b.

Now we perform the same statistics for the zeros of other Dirichlet  $L$ -functions  $L_\chi$ . We perform the statistics for the deltas of 1 million zeros, for deltas in  $[0, 100]$ , and with precision 0.1. This time we consider a real and a complex non-real character. For a complex non-real character, the associated  $L$ -function is not real analytic, and the zeros are no longer symmetric with respect to the real axes. Therefore we compute the deltas of those with positive imaginary part and the deltas for those with negative imaginary part, and we compute the cumulative result. Since the sequence of zeros is not symmetric with respect to 0, we take the first million zeros in the following sense: We order the zeros by absolute value and we consider the first million of them for the statistics.

The first statistics is for  $\chi = \chi_4$ , the only primitive character of conductor 4. The character  $\chi_4$  is real and the associated Dirichlet function real-analytic. The second statistics is for  $\chi = \chi_{7,3}$ , one of the primitive complex characters of conductor 7. Figures 19 show the histograms of deltas in  $[10, 30]$ . Figures 20 show the histograms of deltas in  $[30, 50]$ . Again we find that the deficit locations coincide with Riemann zeros.

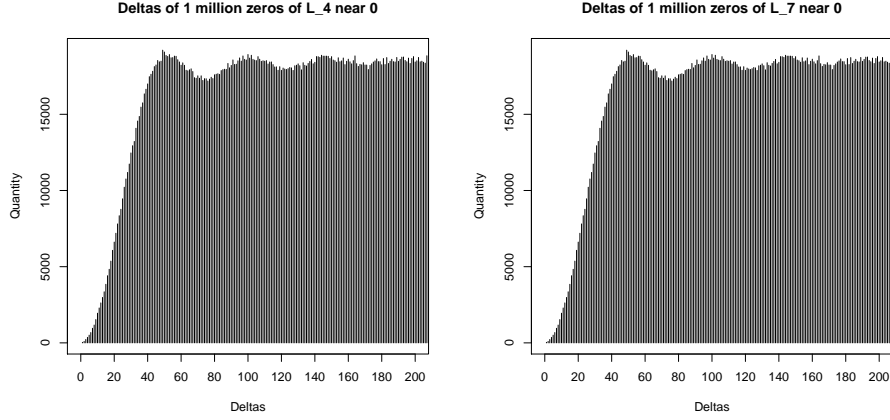


Figures 19.a and 19.b.



Figures 20.a and 20.b.

We analyze next the distribution of deltas near 0. We plot the histogram near 0 of the deltas of 1 million zeros with precision 0.01. We observe the predicted GUE pair correlation distribution as pictures 21 show.



Figures 21.a and 21.b.

**Eñe product explanation.**

We note that for a real character  $\chi$ ,

$$\bar{L}_\chi(s) = \overline{L_\chi(\bar{s})} = L_\chi(s) .$$

The eñe product explanation of the first numerical result for  $\chi_3$  is based on the following computation (where we denote by  $\chi_0$  the principal character modulo 3)

$$\begin{aligned}
 L_{\chi_3} \bar{\star} \bar{L}_{\chi_3} &= L_{\chi_3} \bar{\star} L_{\chi_3} \\
 &= \left( \prod_p (1 - \chi_3(p)p^{-s})^{-1} \right) \bar{\star} \left( \prod_q (1 - \chi_3(q)q^{-s})^{-1} \right) \\
 &= \prod_p (1 - \chi_3(p)p^{-s})^{-1} \bar{\star} (1 - \chi_3(p)p^{-s})^{-1} \\
 &= \prod_p (1 - \chi_3(p)^2 p^{-1/2} p^{-s}) \\
 &= \prod_p (1 - \chi_0(p)p^{-1/2-s}) \\
 &= (1 - 3^{-1/2-s})^{-1} \prod_p (1 - p^{-1/2-s}) \\
 &= (1 - 3^{-1/2-s})^{-1} \zeta(s + 1/2)^{-1} .
 \end{aligned}$$

In general, for an arbitrary character  $\chi$  modulo  $n$ , we recognize the distribution of the deltas of the zeros of  $L_\chi$  in the result of the eñe product of  $L_\chi$  with  $\bar{L}_\chi$ . We have

$$\bar{L}_\chi = L_{\bar{\chi}} .$$

Also observe that

$$\chi \cdot \bar{\chi} = |\chi|^2 = \chi_0 ,$$

where  $\chi_0$  is the principal character modulo  $n$ .

Therefore we have

$$\begin{aligned} L_\chi \bar{\chi} \bar{L}_\chi &= L_\chi \bar{\chi} L_{\bar{\chi}} \\ &= \left( \prod_{p|n} (1 - \chi(p)p^{-s})^{-1} \right) \bar{\chi} \left( \prod_{q|n} (1 - \bar{\chi}(q)q^{-s})^{-1} \right) \\ &= \prod_p (1 - \chi(p)p^{-s})^{-1} \bar{\chi} (1 - \bar{\chi}(p)p^{-s})^{-1} \\ &= \prod_p (1 - |\chi(p)|^2 p^{-1/2} p^{-s}) \\ &= \prod_p (1 - \chi_0(p) p^{-1/2-s}) \\ &= \prod_{p|n} (1 - p^{-1/2-s})^{-1} \cdot \prod_p (1 - p^{-1/2-s}) \\ &= \zeta(s + 1/2)^{-1} \prod_{p|n} (1 - p^{-1/2-s})^{-1} . \end{aligned}$$

Observe that the zeros of each Euler factor

$$f_p(s) = (1 - p^{-1/2-s})^{-1}$$

are for  $k \in \mathbb{Z}$ ,

$$s_k = -\frac{1}{2} + i \frac{2\pi}{\log p} k .$$

According to the explanation with the eñe product, we should observe a deficit of deltas (with a lower order amplitude) near locations multiples of the fundamental harmonic

$$\frac{2\pi}{\log p} k$$

for  $k \in \mathbb{Z}$ .

For  $p = 2$ ,  $p = 3$  and  $p = 7$  we have,

$$\frac{2\pi}{\log 2} = 9.0647\dots$$

$$\frac{2\pi}{\log 3} = 5.7192\dots$$

$$\frac{2\pi}{\log 7} = 3.2289\dots\dots$$

A good eye can spot a trace of these deficit locations in the figures 16, 17, 19 and 20. In particular comparing these figures with figures 3 and 4.

### Script.

We provide the script for computing the deltas of the zeros of a complex non-real L-function since it is slightly different from the previous ones. Here we feed the program by reading into Rubinstein's table "zeros-0007-2000000" which contains the first zeros for each of the three primitive characters of conductor 7. The zeros for the complex character that we are considering are those after row 2 000 000.

```
zeros<-read.table("zeros-0007-2000000",skip=2000000,nrows=1000000)
z<-zeros[,3]
z.plus<-z[z>0]
z.minus<--z[z<0]
x=rep(0,10000)
zeta1<-z.plus
zeta2<-z.minus
N=length(z.plus)
k=0
for (i in 1:N)
{
while( ((zeta1[i]-zeta2[i+k])<100.01) & (k+i >1) )
{
k<-k-1
}
k=k+1
j=k
while ( (zeta1[i]-zeta2[i+j]>0) & (zeta1[i]-zeta2[i+j]<5.01) )
```

```

{
d=100*(zeta1[i]-zeta2[i+j])
x[as.integer(d)]=x[as.integer(d)]+1
j=j+1
}
}
zeta1=numeric()
zeta2=numeric()
zeta1<-z.minus
zeta2<-z.minus
N=length(z.minus)
k=0
for (i in 1:N)
{
while( ((zeta1[i]-zeta2[i+k])<100.01) & (k+i >1) )
{
k<-k-1
}
k=k+1
j=k
while ( (zeta1[i]-zeta2[i+j]>0) & (zeta1[i]-zeta2[i+j]<5.01) )
{
d=100*(zeta[i]-zeta3[i+j])
x[as.integer(d)]=x[as.integer(d)]+1
j=j+1
}
}
}

```

##### 5. ZEROS OF $L$ -FUNCTIONS REPLICATE FROM THEIR MATING WITH RIEMANN ZEROS.

We present in this section and the next one a new type of statistics. We do study the statistics of differences of zeros of an  $L$ -function  $L_{\chi_1}$  with the zeros of another  $L$ -function  $L_{\chi_2}$ . We name this operation the "mating" of zeros of  $L_{\chi_1}$  and  $L_{\chi_2}$ . As

predicted by the eñe product theory, it appears that the sequence of Riemann zeros plays the role of the unit for this mating operation. More precisely, the statistics of this section verify that the mating of Riemann zeros with those of another  $L$ -function  $L$  yield as deficit values the zeros of  $L$  itself.

We perform the statistics mating the Riemann zeros with the zeros of  $L_{\chi_3}$  where  $\chi_3$  is as before the only primitive character of conductor 3. The function  $L_{\chi_3}$  is real analytic and its zeros are symmetric with respect to the real axes. We consider only the non-real (i.e. non-trivial) zeros with positive imaginary part. We denote by  $(1/2 + i\gamma_i^{(3)})_{i \geq 1}$ , or simply  $(\gamma_i^{(3)})_{i \geq 1}$ , the zeros of  $L_{\chi_3}$ , with  $i \mapsto \gamma_i^{(3)}$  increasing.. The first 18 ones, less than 51, are the following

$$\gamma_1^{(3)} = 8.039737156 \dots$$

$$\gamma_2^{(3)} = 11.24920621 \dots$$

$$\gamma_3^{(3)} = 15.70461918 \dots$$

$$\gamma_4^{(3)} = 18.2619975 \dots$$

$$\gamma_5^{(3)} = 20.45577081 \dots$$

$$\gamma_6^{(3)} = 24.05941486 \dots$$

$$\gamma_7^{(3)} = 26.57786874 \dots$$

$$\gamma_8^{(3)} = 28.21816451 \dots$$

$$\gamma_9^{(3)} = 30.74504026 \dots$$

$$\gamma_{10}^{(3)} = 33.89738893 \dots$$

$$\gamma_{11}^{(3)} = 35.60841265 \dots$$

$$\gamma_{12}^{(3)} = 37.55179656 \dots$$

$$\gamma_{13}^{(3)} = 39.48520726 \dots$$

$$\gamma_{14}^{(3)} = 42.61637923 \dots$$

$$\gamma_{15}^{(3)} = 44.12057291 \dots$$

$$\gamma_{16}^{(3)} = 46.27411802 \dots$$

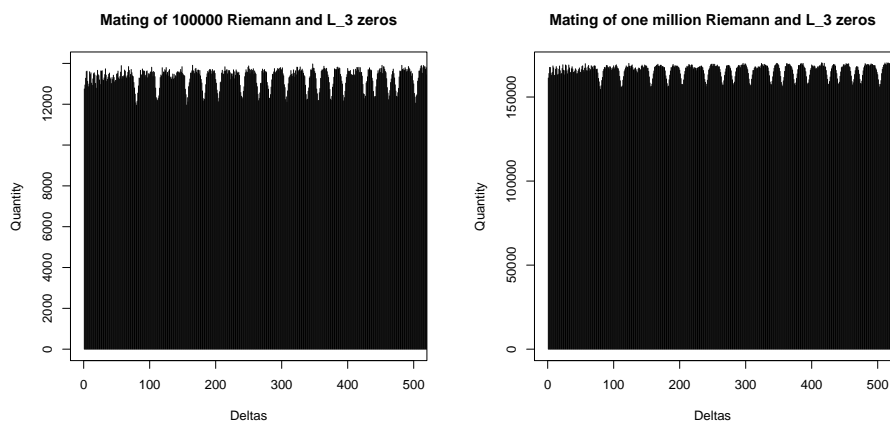
$$\gamma_{17}^{(3)} = 47.51410451 \dots$$

$$\gamma_{18}^{(3)} = 50.37513865 \dots$$

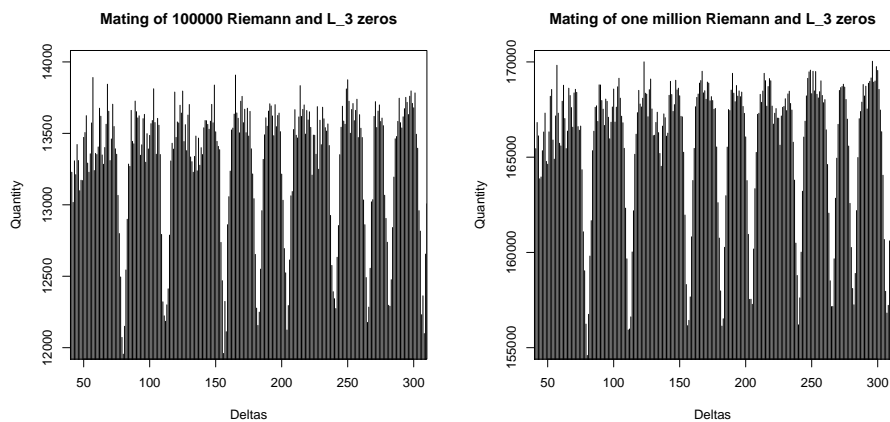
This time the "deltas" are differences

$$\delta_{i,j} = \gamma_i - \gamma_j^{(3)} .$$

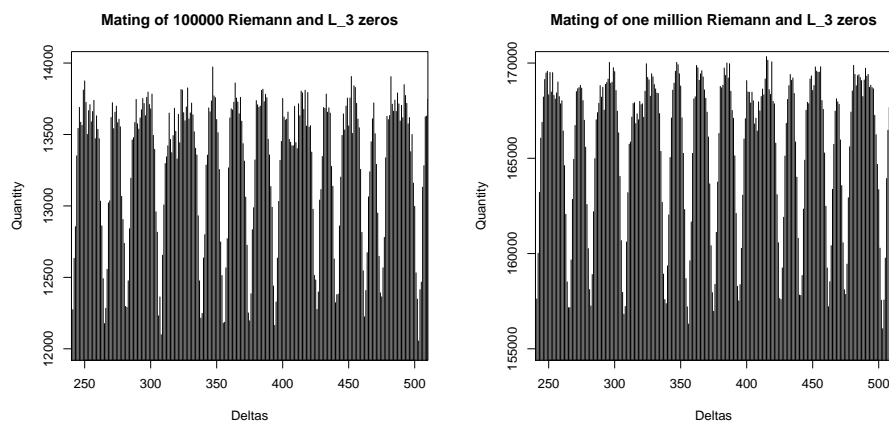
We perform statistics (a) with  $1 \leq i, j \leq 100\,000$  and statistics (b) with  $1 \leq i, j \leq 10^6$ . We look at deltas in  $[0, 50]$  with precision 0.1. The results are presented in the following figures.



Figures 22.a and 22.b.



Figures 23.a and 23.b.



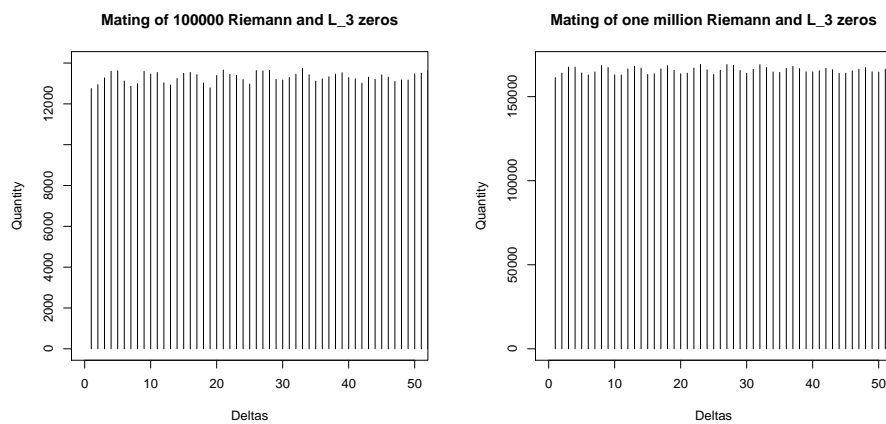
Figures 24.a and 24.b.

We observe that this time the deficient locations for the deltas happen exactly at the location of the zeros of  $L_{\chi_3}$ . We easily recognize in figures 23.a and 23.b the location of the first zeros of  $L_{\chi_3}$ . We can check the full list of zeros less than 50 by looking also at the figures 24.a and 24.b. We conclude that the zeros of  $L$ -functions replicate mating them with Riemann zeros.

A new feature is that near 0 we no longer have a GUE distribution for the deltas. As the theory of the eñe product explains, the deficit at 0 only occurs when we have symmetric zeros, i.e. we mate the zeros of  $L_{\chi_1}$  with those of  $L_{\chi_2}$  when

$$\chi_1 = \bar{\chi}_2 ,$$

and we have an atomic mass at 0 that comes from the sum of symmetric zeros of  $L_{\chi_1}$  and  $L_{\bar{\chi}_1}$ . Thus if the character is not real, then we don't have a GUE distribution, not even a deficit, but the Riemann Hypothesis is still conjectured, thus there is no direct relation between the Riemann Hypothesis and Montgomery Conjecture. The author knows no reference in the literature for this observation.



Figures 25.a and 25.b.

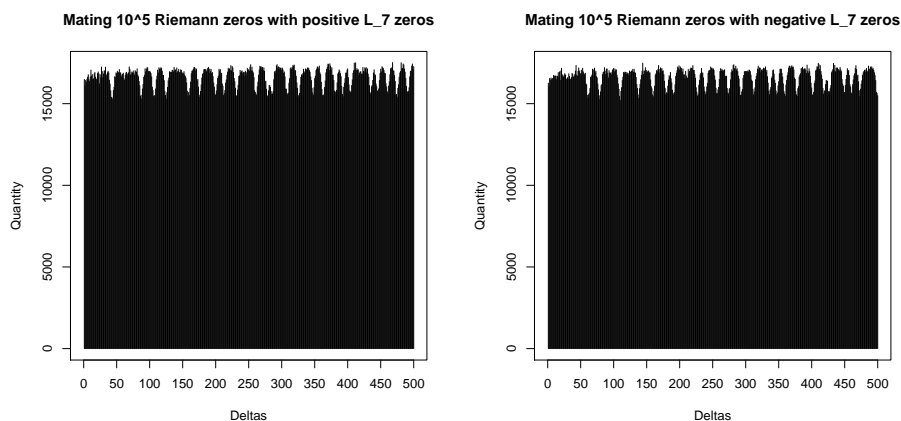
Next we perform the same mating statistics of Riemann zeros with zeros of  $L_{\chi_{7,3}}$ . Recall that the zeros of this non-real analytic  $L$ -functions are not symmetric with respect to 0. We perform two statistics. We consider the first 100 000 Riemann zeros and compute all deltas with positive (resp. negative taking their negative value) zeros of  $L_{\chi_{7,3}}$ . The list of the first positive zeros of  $L_{\chi_{7,3}}$  less than 50 are

$$\begin{aligned}
\gamma_1^{(7+)} &= 4.356402\dots \\
\gamma_2^{(7+)} &= 8.785555\dots \\
\gamma_3^{(7+)} &= 10.736120\dots \\
\gamma_4^{(7+)} &= 12.532548\dots \\
\gamma_5^{(7+)} &= 15.937448\dots \\
\gamma_6^{(7+)} &= 17.616053\dots \\
\gamma_7^{(7+)} &= 20.030559\dots \\
\gamma_8^{(7+)} &= 21.314647\dots \\
\gamma_9^{(7+)} &= 23.203672\dots \\
\gamma_{10}^{(7+)} &= 26.169945\dots \\
\gamma_{11}^{(7+)} &= 27.873375\dots \\
\gamma_{12}^{(7+)} &= 28.599794\dots \\
\gamma_{13}^{(7+)} &= 30.919561\dots \\
\gamma_{14}^{(7+)} &= 32.610089\dots \\
\gamma_{15}^{(7+)} &= 34.792503\dots \\
\gamma_{16}^{(7+)} &= 36.344756\dots \\
\gamma_{17}^{(7+)} &= 38.206755\dots \\
\gamma_{18}^{(7+)} &= 39.338483\dots \\
\gamma_{19}^{(7+)} &= 40.476472\dots \\
\gamma_{20}^{(7+)} &= 43.539481\dots \\
\gamma_{21}^{(7+)} &= 44.595772\dots \\
\gamma_{22}^{(7+)} &= 46.096099\dots \\
\gamma_{23}^{(7+)} &= 47.491559\dots \\
\gamma_{24}^{(7+)} &= 49.126475\dots \\
&\vdots
\end{aligned}$$

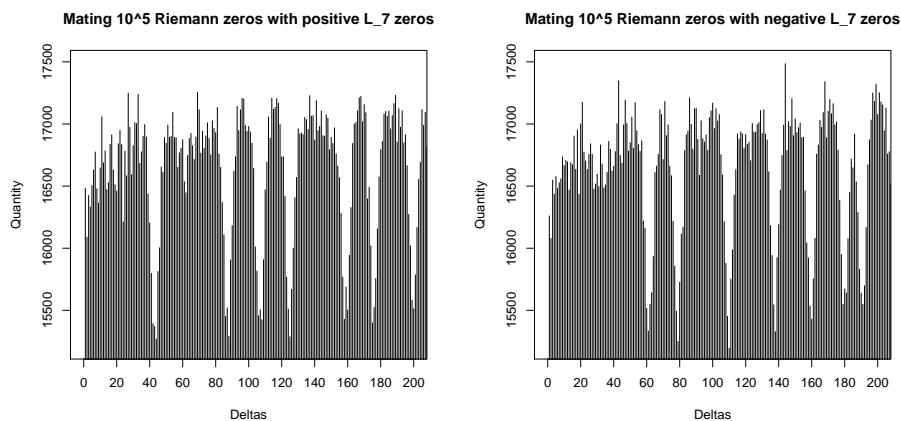
The list of the first negative zeros of  $L_{\chi_{7,3}}$  less than 51 are

$$\begin{aligned}\gamma_1^{(7-)} &= 6.201230\dots \\ \gamma_2^{(7-)} &= 7.927431\dots \\ \gamma_3^{(7-)} &= 11.010445\dots \\ \gamma_4^{(7-)} &= 13.829868\dots \\ \gamma_5^{(7-)} &= 16.013727\dots \\ \gamma_6^{(7-)} &= 18.044858\dots \\ \gamma_7^{(7-)} &= 19.113886\dots \\ \gamma_8^{(7-)} &= 22.756406\dots \\ \gamma_9^{(7-)} &= 23.955938\dots \\ \gamma_{10}^{(7-)} &= 25.723104\dots \\ \gamma_{11}^{(7-)} &= 27.455596\dots \\ \gamma_{12}^{(7-)} &= 29.338505\dots \\ \gamma_{13}^{(7-)} &= 31.284265\dots \\ \gamma_{14}^{(7-)} &= 33.672299\dots \\ \gamma_{15}^{(7-)} &= 34.774195\dots \\ \gamma_{16}^{(7-)} &= 35.973150\dots \\ \gamma_{17}^{(7-)} &= 37.786921\dots \\ \gamma_{18}^{(7-)} &= 40.224566\dots \\ \gamma_{19}^{(7-)} &= 41.909138\dots \\ \gamma_{20}^{(7-)} &= 42.712631\dots \\ \gamma_{21}^{(7-)} &= 44.977200\dots \\ \gamma_{22}^{(7-)} &= 46.086774\dots \\ \gamma_{23}^{(7-)} &= 47.348801\dots \\ \gamma_{24}^{(7-)} &= 50.017326\dots \\ &\vdots\end{aligned}$$

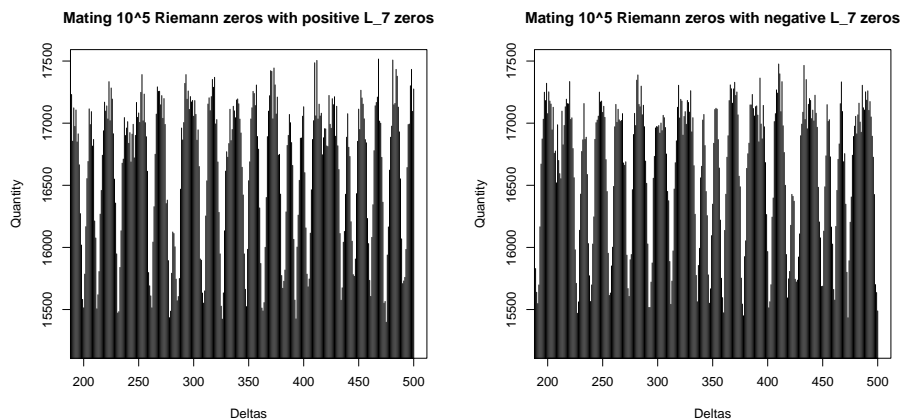
The following figures show the result of the numerical statistics. Figures (a), resp. (b), are for the mating against positive, resp. negative, zeros. We observe for statistics (a) that the deficient locations do correspond to values of the positive zeros. For statistics (b) we observe these locations at the values of the negative zeros. In particular in figures 27 we appreciate the location of the first zeros.



Figures 26.a and 26.b.

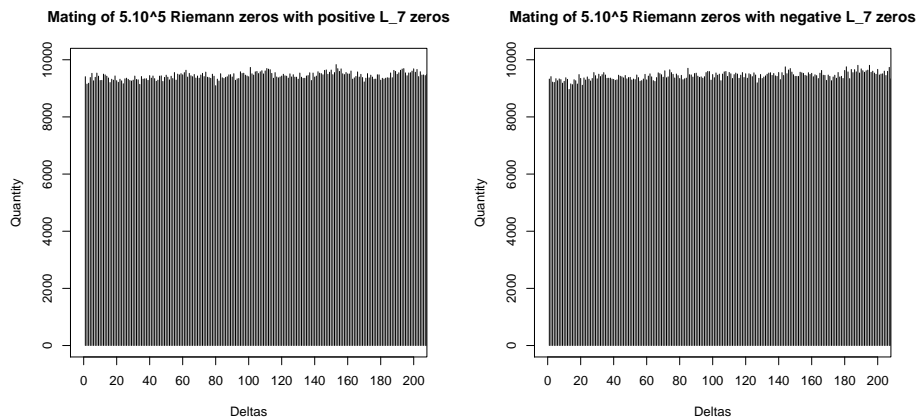


Figures 27.a and 27.b.



Figures 28.a and 28.b.

We perform a final statistic in order to check the nonexistence of the GUE distribution, and not even a deficit of deltas effect near 0. We compute the deltas near 0 against half million Riemann zeros with precision 0.01. The results are shown in Figures 29, figure 29.a for positive deltas and figure 29.b for negative ones. Figures 29 show the deltas with double precision in the range  $[0, 2]$ . The reader can compare directly these figures with Figures 21.c and 21.d. The conclusion is clear: No GUE distribution near 0.



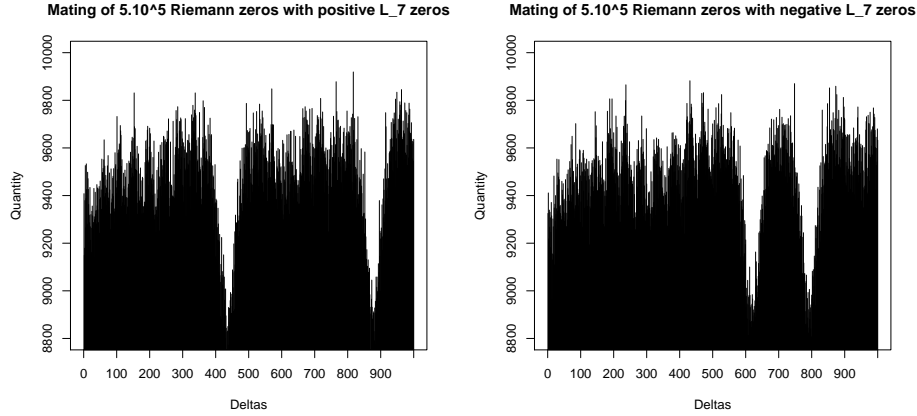
Figures 29.a and 29.b.

We check also from these statistics the location with double precision the first positive and negative zero in figures 30.a and 30.b which show the deltas in the range  $[0, 10]$  with double precision. We can appreciate distinctly with double precision in figure 30.a both positive zeros less than 10

$$\gamma_1^{(7+)} = 4.356402\dots \quad \gamma_2^{(7+)} = 8.785555\dots$$

and in figure 30.b both "negative" zeros less than 10

$$\gamma_1^{(7-)} = 6.201230\dots \quad \gamma_2^{(7-)} = 7.927431\dots$$



Figures 30.a and 30.b.

### Eñe product explanation.

The computation follows. We have for any Dirichlet  $L_\chi$ ,

$$\begin{aligned} L_\chi \bar{\chi} \bar{\zeta} &= L_\chi \bar{\chi} \bar{\zeta} \\ &= \prod_p (1 - \chi(p)p^{-s})^{-1} \bar{\star} \prod_q (1 - q^{-s})^{-1} \\ &= \prod_p (1 - \chi(p)p^{-s})^{-1} \bar{\star} (1 - p^{-s})^{-1} \\ &= \prod_p (1 - \chi(p)p^{-1/2}p^{-s}) \\ &= \prod_p (1 - \chi(p)p^{-(s+1/2)}) \\ &= L_\chi (s + 1/2)^{-1} . \end{aligned}$$

Therefore we recognize that the mating of zeros of  $L_\chi$  with Riemann zeros has deficient deltas at the location corresponding to the imaginary part of zeros of  $L_\chi$ .

### Scripts.

Below is the script we used in order to produce the previous figures. The script is slightly different from previous ones since we compute separately positive and negative zeros. The cumulative positive deltas are stored in the list "x" and the negative in the

list "y". The zeros of Dirichlet  $L$ -function of conductor 7 are stored in Rubinstein's file "zeros-0007-2000000", and Riemann zeros are from Rubinstein's file "zeros-0001-35161820".

```

zerosL<-read.table("zeros-0007-2000000",skip=2000000,nrows=1000000)
z<-zerosL[,3]
z.plus<-z[z>0]
z.minus<--z[z<0]
zerosR<-scan("zeros-0001-35161820",skip=0,nlines=100000)
x=rep(0,500)
zeta1<-zerosR
zeta2<-z.minus
N=length(zeta) j=1
for (i in 1:N)
{
while ( (zeta1[i]-zeta2[j])>50.1 )
{
j=j+1
}
l=0
while ( ((zeta1[i]-zeta2[j+1])>0) & ((zeta1[i]-zeta2[j+1])<50.1) )
{
d=10*(zeta1[i]-zeta2[j+1])
x[as.integer(d)]=x[as.integer(d)]+1
l=l+1
}
}
y=rep(0,500)
zeta1<-zerosR
zeta3<-z.plus
N=length(zeta)
j=1
for (i in 1:N)

```

```

{
while ( (zeta1[i]-zeta3[j])>50.1 )  j=j+1
l=0
while ( ((zeta1[i]-zeta3[j+1])>0) & ((zeta1[i]-zeta3[j+1])<50.1) )
{
d=10*(zeta1[i]-zeta3[j+1])
y[as.integer(d)]=y[as.integer(d)]+1
l=l+1
}
}

```

## 6. MATING OF GENERAL $L$ -FUNCTIONS.

In this section we perform similar statistics to those in the previous section but mating the zeros of two Dirichlet  $L$ -functions  $L_{\chi_1}$  and  $L_{\chi_2}$ . This time we observe that the deficient locations for the statistics of deltas correspond to the zeros of an arithmetically well determined, namely  $L_{\chi_1\bar{\chi}_2}$ .

For a character  $\chi$  we denote by  $f_\chi$  its conductor. We have

$$f_{\bar{\chi}} = f_\chi .$$

All characters considered are primitive, i.e. defined modulo its conductor. Let  $\chi_1$  and  $\chi_2$  be two characters. If  $f_{\chi_1} \wedge f_{\chi_2} = 1$  then the conductor of  $\chi_1\bar{\chi}_2$  is

$$f_{\chi_1\bar{\chi}_2} = f_{\chi_1} \cdot f_{\chi_2} .$$

The first complex non-real Dirichlet character has conductor 5. Therefore the mating of two Dirichlet  $L$ -functions of complex non-real characters with distinct conductors has conductor at least 35. We have only access to Rubinstein's public data that contains large files of zeros for Dirichlet  $L$ -functions with conductor  $\leq 19$ . Therefore we limit our numerical computation to real characters for which we can check the result with the available data. This is done only for checking purposes. Note that we could indeed compute, with a rough precision, the zeros of higher conductor Dirichlet  $L$ -functions (for example 35) by using Rubinstein's data of conductors  $\leq 19$ .

We choose to mate the zeros of Dirichlet  $L$ -functions  $L_{\chi_3}$  of conductor 3, and  $L_{\chi_4}$  of conductor 4. We should obtain the zeros of the only Dirichlet  $L$ -function of conductor 12,  $L_{\chi_{12}}$ . The list of the first zeros of  $L_{\chi_{12}}$  less than 50 is

$$\gamma_1^{(12)} = 3.8046276331 \dots$$

$$\gamma_2^{(12)} = 6.6922233205 \dots$$

$$\gamma_3^{(12)} = 8.8905929587 \dots$$

$$\gamma_4^{(12)} = 11.188392745 \dots$$

$$\gamma_5^{(12)} = 12.966178808 \dots$$

$$\gamma_6^{(12)} = 15.181480876 \dots$$

$$\gamma_7^{(12)} = 16.632633275 \dots$$

$$\gamma_8^{(12)} = 18.884369457 \dots$$

$$\gamma_9^{(12)} = 20.103928191 \dots$$

$$\gamma_{10}^{(12)} = 22.285839107 \dots$$

$$\gamma_{11}^{(12)} = 23.561319713 \dots$$

$$\gamma_{12}^{(12)} = 25.411633892 \dots$$

$$\gamma_{13}^{(12)} = 27.013943986 \dots$$

$$\gamma_{14}^{(12)} = 28.442203258$$

$$\gamma_{15}^{(12)} = 30.204006556 \dots$$

$$\gamma_{16}^{(12)} = 31.648077615 \dots$$

$$\gamma_{17}^{(12)} = 33.03713288 \dots$$

$$\gamma_{18}^{(12)} = 35.027378485 \dots$$

$$\gamma_{19}^{(12)} = 35.778044577 \dots$$

$$\gamma_{20}^{(12)} = 37.926816821 \dots$$

$$\gamma_{21}^{(12)} = 38.973998822 \dots$$

$$\gamma_{22}^{(12)} = 40.484154751 \dots$$

$$\gamma_{23}^{(12)} = 42.235143018 \dots$$

$$\gamma_{24}^{(12)} = 43.192847103 \dots$$

$$\gamma_{25}^{(12)} = 44.948822502 \dots$$

$$\gamma_{26}^{(12)} = 46.243369979 \dots$$

$$\gamma_{27}^{(12)} = 47.646400501 \dots$$

$$\gamma_{28}^{(12)} = 48.943728012 \dots$$

$$\vdots$$

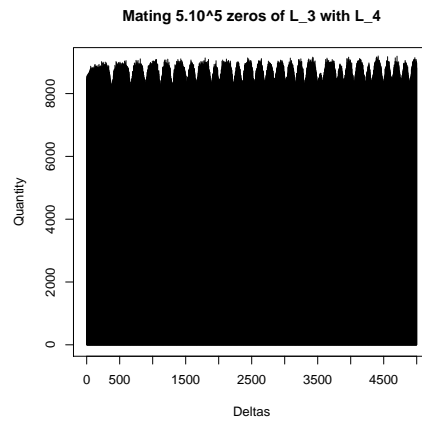


Figure 31.

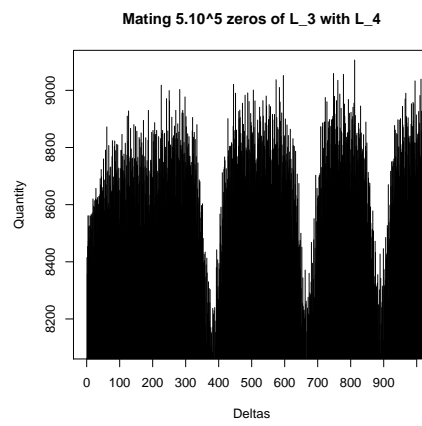


Figure 32.

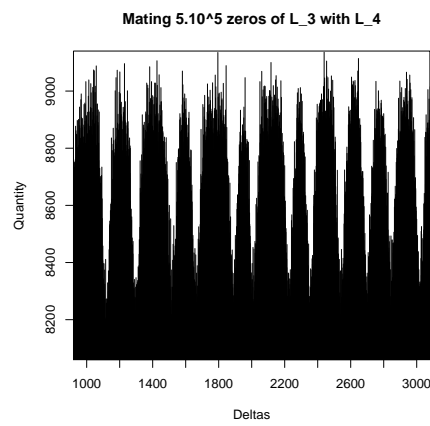


Figure 33.

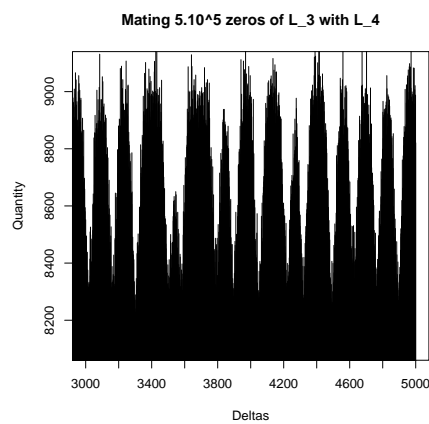


Figure 34.

Again in this situation there is no GUE distribution near 0 since the zeros of  $L_{\chi_3}$  and  $L_{\chi_4}$  are not symmetric. Figure 35 shows the histogram of the deltas in the range  $[0, 2]$  with precision 0.01. This figure is to be compared to figures 21.

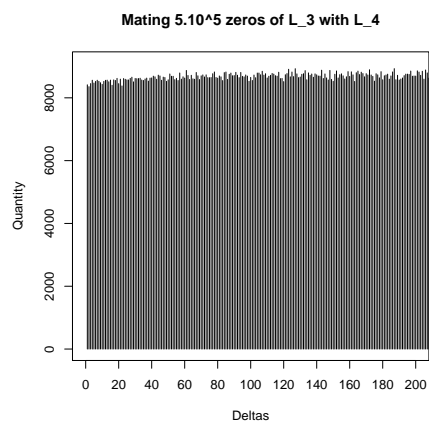


Figure 35.

**Eñe product explanation.**

The computation follows. We have for any pair of Dirichlet  $L$ -function  $L_{\chi_1}$  and  $L_{\chi_2}$ ,

$$\begin{aligned}
L_{\chi_1} \bar{\star} \bar{L}_{\chi_2} &= L_{\chi_1} \bar{\star} L_{\bar{\chi}_2} \\
&= \prod_p (1 - \chi_1(p)p^{-s})^{-1} \bar{\star} \prod_q (1 - \bar{\chi}_2(q)q^{-s})^{-1} \\
&= \prod_p (1 - \chi_1(p)p^{-s})^{-1} \bar{\star} (1 - \bar{\chi}_2(p)p^{-s})^{-1} \\
&= \prod_p (1 - (\chi_1 \bar{\chi}_2)(p)p^{-1/2}p^{-s}) \\
&= \prod_p (1 - (\chi_1 \bar{\chi}_2)(p)p^{-(s+1/2)}) \\
&= L_{\chi \bar{\chi}_2}(s + 1/2)^{-1}
\end{aligned}$$

## 7. MATING WITH LOCAL EULER FACTORS.

In this section we study the mating of  $L$ -functions with local Euler factors. We mate the positive imaginary part of Riemann zeros with the sequence of positive imaginary part of zeros of Euler factor

$$f_p(s) = (1 - p^{-s}) ,$$

which is the arithmetic sequence

$$\gamma_k^{(p)} = \frac{2\pi}{\log(p)} k ,$$

with  $k \in \mathbb{Z}$ .

More generally we can consider the mating with general Euler Dirichlet local factors

$$f_{p,\chi}(s) = (1 - \chi(p)p^{-s}) ,$$

but we restrict the numerical statistics to Riemann Euler local factors.

In order to have a substantial number of deltas we need to work with a very large file of Riemann zeros because this time the arithmetical sequence of Euler zeros has constant density. For a given number of Riemann zeros we pick more deltas if the prime  $p$  is large. For this reason, with our limited data of zeros available, we run the statistics for  $p = 23$ ,

$$\frac{2\pi}{\log(23)} = 2.00389 \dots ,$$

and the first 10 million Riemann zeros (statistics (a)); and for  $p = 67$ ,

$$\frac{2\pi}{\log(67)} = 1.494327 \dots ,$$

and the first 15 million of Riemann zeros (statistics (b)).

The histograms obtained (figures below for different ranges of deltas) show a uniform distribution with deficit locations at the corresponding Euler zeros, for  $k \in \mathbb{Z}$ ,

$$\gamma_k^{(p)} = \frac{2\pi}{\log(p)} k.$$

The deficit of deltas at these locations can also be seen for statistics with smaller values of  $p$ , but because of the "small" number of Riemann zeros at our disposition, the statistics is too poor <sup>1</sup>

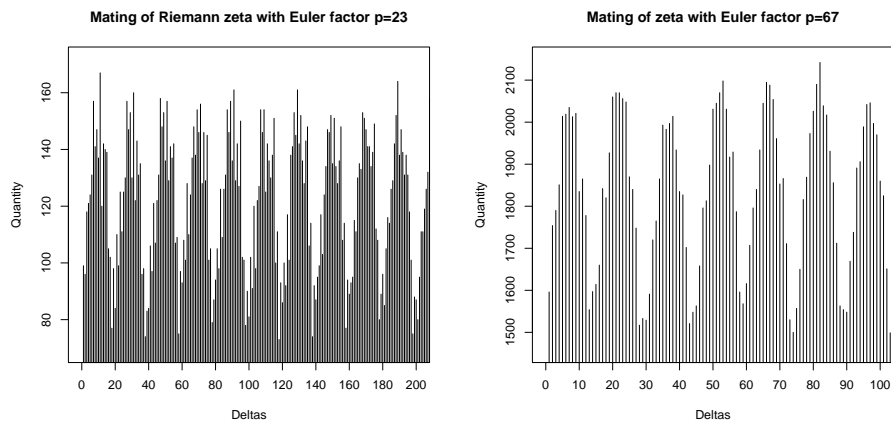


Figure 36.a and 36.b.

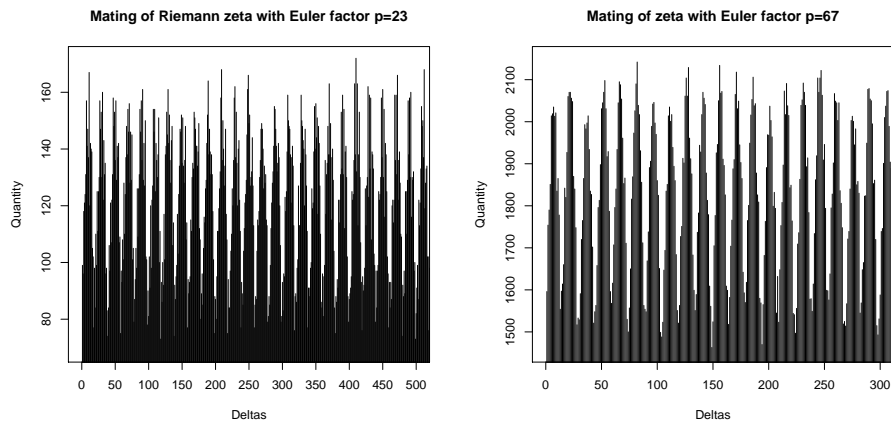


Figure 37.a and 37.b.

---

<sup>1</sup>Also our laptop has a RAM memory of 512 Mb which does not allow R to read a vector with more than 20 million Riemann zeros.

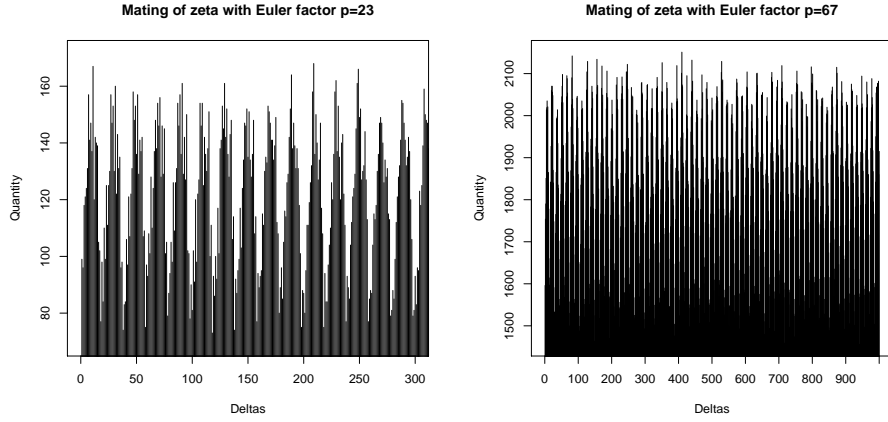


Figure 38.a and 38.b.

### Eñe product explanation.

We have

$$\begin{aligned}
 \zeta \bar{\star} \bar{f}_p &= \zeta \bar{\star} f_p \\
 &= \prod_q (1 - q^{-s})^{-1} \bar{\star} (1 - p^{-s})^{-1} \\
 &= (1 - p^{-s})^{-1} \bar{\star} (1 - p^{-s})^{-1} \\
 &= (1 - p^{-s}) \bar{\star} (1 - p^{-s}) \\
 &= (1 - p^{-1/2} p^{-s}) \\
 &= f_p(s + 1/2) .
 \end{aligned}$$

We have in general for an arbitrary Dirichlet  $L$ -function:

$$\begin{aligned}
 L_\chi \bar{\star} \bar{f}_p &= L_\chi \bar{\star} f_p \\
 &= \prod_q (1 - \chi(q) q^{-s})^{-1} \bar{\star} (1 - p^{-s})^{-1} \\
 &= (1 - \chi(p) p^{-s})^{-1} \bar{\star} (1 - p^{-s})^{-1} \\
 &= (1 - \chi(p) p^{-1/2} p^{-s}) \\
 &= f_{p,\chi}(s + 1/2) .
 \end{aligned}$$

8. FINE STRUCTURE OF DELTAS NEAR 0.

We come back in this section to analyze the fine structure of the statistics of deltas near 0.

As we have observed, Montgomery conjecture is verified numerically for the deltas of zeros of arbitrary  $L$ -functions, but not for the mating of zeros of non-conjugate  $L$ -functions. As explained, the GUE distribution arises because of the symmetry of the zeros mated, i.e. it is a genuine real-analytic phenomenon.

For the Riemann zeta function, the eñe product analysis of the distribution of deltas near zero reveals that after the first order GUE correction, we have a second order term corresponding to the pole of  $\zeta(s + 1/2)$  at  $s = 0$ . This yields a positive Fresnel distribution.

We verify numerically this first order correction to the GUE distribution. In the numerical application we consider the deltas of 5 million Riemann zeros. These have imaginary part less than  $T_0$  for  $T_0 = 2\,630\,122$ . We consider the frequency

$$\omega_0 = \frac{1}{2\pi} \log T_0 = 0.02352714\dots$$

We correct the histogram of the deltas by adding a GUE density

$$t \mapsto A \left( \frac{\sin(\pi\omega_0 t)}{\pi\omega_0 t} \right)^2 .$$

Figure 39 shows the distribution of the deltas and figure 40 the corrected distribution of the deltas showing the Fresnel distribution (both in the range  $[0, 2]$ ). Figures 41 and 42 show the same data in the range  $[0, 6]$  for a better view of the queue. We have adjusted the coefficient  $A$  in order to fit the best with a Fresnel distribution looking at the first minima and the second maximum.

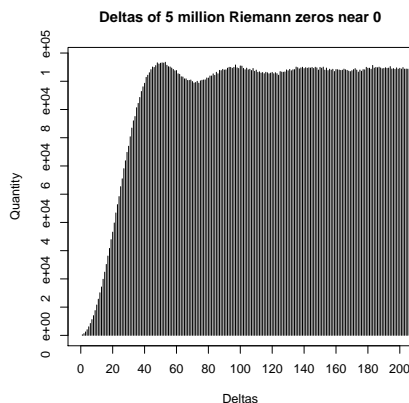


Figure 39.

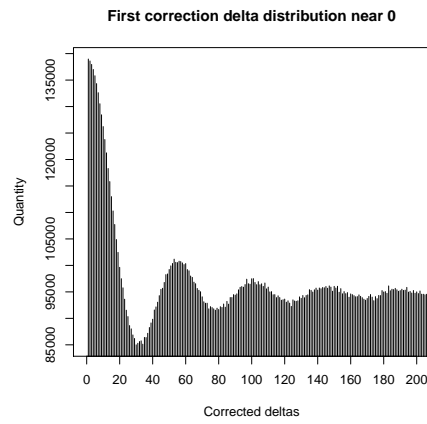


Figure 40.

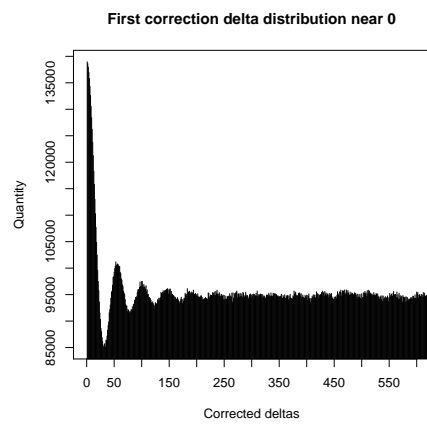


Figure 41.

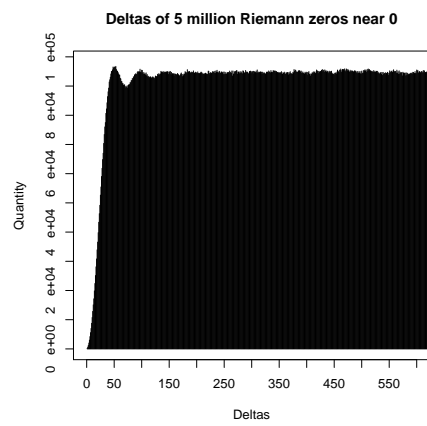


Figure 42.

**Script.**

We have previously stored the result of computing the deltas of 5 million Riemann zeros in the range  $[0, 200]$  with precision 0.01. The variable  $x$  contains the cumulative count of deltas with the stated precision. Note also that  $\pi \cdot \omega_0 / 100 = 0.0739127\dots$

```
load("data 5 million")
correction=numeric()
for (k in 1:200000) correction[k]=139000*(sin(0.0739127*k)/(0.0739127*k))^2
x1<-x+correction
barplot(x1)
```

## REFERENCES

- [Bo] BOMBIERI, E., *Problems of the Millenium: The Riemann Hypothesis*, [www.claymath.org](http://www.claymath.org), Official problem description.
- [Co] CONREY, J.B., *The Riemann Hypothesis*, Notices of the AMS, March 2003, p.341-353.
- [KS] KATZ, N.M.; SARNAK, P., *Random matrices, Frobenius eigenvalues, and monodromy*, AMS Colloquium Publications, **45**, AMS, Providence RI, 1999.
- [Mo1] MONTGOMERY, H.L., *The pair correlations of zeros of the zeta function*, *Analytic Number Theory*, editor H.G. Diamond, Proc. Symp. Pure Math., Providence, 1973, p.181-193.
- [Mo2] MONTGOMERY, H.L., *Distribution of the Zeros of the Riemann Zeta function*, Proc. ICM, Vancouver, 1974, p.379-381.
- [Od] ODLYZKO, A.M. [www.dtc.umn.edu/~odlyzko](http://www.dtc.umn.edu/~odlyzko), Personal web page.
- [PM1] PÉREZ MARCO, R., *The eñe product*, Manuscript.
- [PM2] PÉREZ MARCO, R., *Eñe product and Riemann zeta function*, Manuscript.
- [Ri1] RIEMANN, B., *Ueber die Anzahl der Primzahlen unter einer gegebenen Grösse*, Monat. der Königl. Preuss. Akad. der Wissen. zu Berlin aus der Jahre, 1859 (1860), p.671-680; Gessam-melte math. Werke und wissensch. Nachlass, 2 Aufl. 1892, p.145-155.
- [Ri2] RIEMANN, B., *Original manuscripts related to [Ri1]*, Scan available at [www.claymath.org](http://www.claymath.org).
- [Ru] RUBINSTEIN, M., [pmmac03.math.uwaterloo.ca/~mrubinst/L\\_function\\_public/ZEROS](http://pmmac03.math.uwaterloo.ca/~mrubinst/L_function_public/ZEROS), Public web page.

CNRS, LAGA UMR 7539, UNIVERSITÉ PARIS XIII, 99, AVENUE J.-B. CLÉMENT, 93430-VILLETANEUSE, FRANCE

*E-mail address:* [ricardo@math.univ-paris13.fr](mailto:ricardo@math.univ-paris13.fr)